Received: 6 April 2021 | Revised: 28 June 2021 | Accepted: 22 July 2021 | Published on: 19 August 2021

DOI: 10.1002/qj.4138

Quarterly Journal of the Royal Meteorological Society RMetS

RESEARCH ARTICLE

Comparison of kilometre and sub-kilometre scale simulations of a foehn wind event over the Larsen C Ice Shelf, Antarctic Peninsula using the Met Office Unified Model (MetUM)

Andrew Orr[1] | **Amélie Kirchgaessner**[1] | **John King**[1] | **Tony Phillips**[1] | **Ella Gilbert**[2] | **Andrew Elvidge**[3] | **Mark Weeks**[4] | **Alan Gadian**[5] | **Peter Kuipers Munneke**[6] | **Michiel van den Broeke**[6] | **Stuart Webster**[4] | **Daniel McGrath**[7]

[1]British Antarctic Survey, Cambridge, UK

[2]University of Reading, Reading, UK

[3]University of East Anglia, Norwich, UK

[4]Met Office, Exeter, UK

[5]University of Leeds, Leeds, UK

[6]University of Utrecht, Utrecht, Netherlands

[7]Colorado State University, Fort Collins, Colorado, USA

Correspondence
A. Orr, British Antarctic Survey, High Cross, Madingley Road, Cambridge, CB3 0ET, UK.
Email: anmcr@bas.ac.uk

Abstract

A foehn event on 27 January 2011 over the Larsen C Ice Shelf (LCIS), Antarctic Peninsula and its interaction with an exisiting ground-based cold-air pool is simulated using the MetUM atmospheric model at kilometre and sub-kilometre scale grid spacing. Atmospheric model simulations at kilometre grid scales are an important tool for understanding the detailed circulation and temperature structure over the LCIS, especially the occurrence of foehn-induced surface melting, erosion of cold-air pools, and low-level wind jets (so-called foehn jets). But whether there is an improvement/convergence in the model representation of these features at sub-kilometre grid scales has yet to be established. The foehn event was simulated at grid spacings of 4, 1.5 and 0.5 km, with the results compared to automatic weather station and radiosonde measurements. The features commonly associated with foehn, such as a leeside hydraulic jump and enhanced leeside warming, were comparatively insensitive to resolution in the 4 to 0.5 km range, although the 0.5 km simulation shows a slightly sharper and larger hydraulic jump. By contrast, during the event the simulation of fine-scale foehn jets above the cold-air pool showed considerable dependence on grid spacing, although no evidence of convergence at higher resolution. During the foehn event, the MetUM model is characterised by a nocturnal cold bias of around 8 °C and an underestimate of the near-surface stability of the cold-air pool, neither of which improved with increased resolution. This finding identifies a key model limitation, at both kilometre and sub-kilometre scales, to realistically capture the vertical mixing in the boundary layer and its impact on thermodynamics, through either daytime heating from below or the downward penetration of foehn jet winds from above. Detailed model-resolved foehn jet dynamics thus

plays a crucial role in controlling the near-surface temperature structure over the LCIS, as well as sub-grid turbulent mixing.

KEYWORDS

1. Tools and methods: Dynamic/processes, regional and mesoscale modelling, 2. Scale: Mesoscale, 3. Physical phenomenon: Dynamics, 4. Geophysical sphere: Atmosphere, orography (including valleys), 5. Geographic/climatic zone: Polar, 6. Application/context: Climate, 7. boundary layer

1 | INTRODUCTION

The westerly flow that dominates the circulation around Antarctica is substantially modified by the mountainous barrier created by the Antarctic Peninsula (Orr *et al.*, 2004; 2008). The behaviour of stratified airflow in response to any mountain barrier is primarily dependent on the non-dimensional mountain height $\widehat{h} = Nh/U$, where N is the Brunt–Väisälä frequency, h is the mountain height, and U is the speed of the impinging flow perpendicular to the barrier (Smith, 1989). If $\widehat{h} > 1$ then the flow is characterised by nonlinear dynamics, including low-level blocking of upstream air flow below a certain height z_d ($< h$) and flow above the dividing streamline height z_d being vertically deflected over the barrier (Hunt and Snyder, 1980; Bacmeister *et al.*, 1990; Baines and Smith, 1993), often resulting in warm and strong downslope flow over the leeward slopes of the barrier, which are referred to as foehn winds (Smith, 1989). Other nonlinear dynamical behaviour associated with this flow regime are upper-level wave-breaking above the barrier and leeside hydraulic jumps (Smith, 1989). A detailed description of the flow regime/parameter space that characterises the Antarctic Peninsula is given by Orr *et al.* (2008).

The occurrence of foehn winds descending the lee (eastern) side of the Antarctic Peninsula is relatively common (Turton *et al.*, 2018; Wiesenekker *et al.*, 2018; Elvidge *et al.*, 2020) and is crucial in determining the atmospheric conditions over the Larsen C Ice Shelf (LCIS), which is the largest ice shelf on the Antarctic Peninsula and situated on its eastern side. The warm foehn winds can cause near-surface air temperatures to rise above the melting point for sustained periods and thus drive surface melting over the western parts of the LCIS (Grosvenor *et al.*, 2014; Luckman *et al.*, 2014; Elvidge *et al.*, 2015; 2016; 2020; Kuipers Munneke *et al.*, 2018; Wiesenekker *et al.*, 2018; Datta *et al.*, 2019; Kirchgaessner *et al.*, 2019; Turton *et al.*, 2020; Gilbert *et al.*, 2021). This is most common during the summer months when the near-surface air temperature is already around the freezing point due to high insolation and results in a distinct west–east gradient in surface melt intensity (Luckman *et al.*, 2014; Bevan *et al.*, 2018; Gilbert *et al.*, 2021). The LCIS is also affected by narrow and relatively low-level wind jets (in the order of 10 km wide and occurring a few hundred metres above the ice surface) originating from the mouths of leeside inlets, formed by the channelling of foehn winds through gaps in the orography into the inlets, which are referred to as "foehn jets" (Elvidge *et al.*, 2015; 2020).

Foehn-induced melting over the Larsen A and B ice shelves contributed to their recent collapse (1995 and 2002, respectively) due to the ensuing meltwater-driven hydro-fracturing (e.g. Scambos *et al.*, 2000), synchronised by flexural stresses in the ice shelf caused by surface lake drainage (Banwell *et al.*, 2013). This allowed inland glaciers to accelerate and increase ice discharge into the ocean, thus contributing to sea-level rise (Rott *et al.*, 1996). The southward progression of ice-shelf collapse suggests that these mechanisms could perhaps result in the future collapse of the LCIS (Kuipers Munneke *et al.*, 2014; Trusel *et al.*, 2015; Bevan *et al.*, 2017). For example, already in recent decades a strengthening of summertime westerly winds impinging on the Antarctic Peninsula has led to increased vertical deflection of flow over the Peninsula (Marshall *et al.*, 2006; Orr *et al.*, 2008; van Lipzig *et al.*, 2008), resulting in a higher occurrence of foehn winds and a rise in the frequency of surface melting over the LCIS (Cape *et al.*, 2015; Datta *et al.*, 2019).

Over the LCIS the boundary layer is generally more stable in winter months and less stable (or even weakly unstable) in summer months (Kuipers Munneke *et al.*, 2012). One characteristic of the stable boundary layer is the formation of cold-air pools, which are characterised by a layer of stagnant, decoupled, cold air above the surface and an elevated capping inversion. These can form when warm-air advection occurs aloft, as well as from cooling of the surface, or a mixture of both (Whiteman *et al.*, 1999; 2001; Zardi and Whiteman, 2013). King *et al.* (2008) demonstrated that warm air advection, associated with a foehn event, over the cold surface of the LCIS generated a cold-air pool. Existing cold-air pools may also cause the foehn flow to decouple from the surface, resulting in the flow travelling well downstream before connecting with the surface. By contrast, the removal/erosion of cold-air pools can occur due to local turbulent processes

such as daytime heating from below or the downward penetration of moderately strong winds from above, which mixes the warmer air aloft with the colder air below (Zardi and Whiteman, 2013). Therefore, both the descending foehn winds at the base of the Antarctic Peninsula and the low-level foehn jets that extend further over the LCIS offer a mechanism for eroding cold-air pools, resulting in considerable changes to the low-level temperature structure. The dynamic displacement of the cold-air pool by the foehn winds offers a further process that can erode its structure (Flamant *et al.*, 2006). Note that such an environment is distinctively different from the kabatabic wind regime that dominates the climate of Antarctica's sloping ice sheets (van den Broeke *et al.*, 2002).

Much of our understanding of the detailed circulation and temperature structure over the LCIS comes from running regional atmospheric model simulations at high horizontal resolution to accurately resolve the topography and capture the complex dynamics of foehn events. However, as well as this aspect, an additional challenge for the atmospheric models is the turbulent erosion/removal of cold-air pools due to the complex interplay between dynamics and thermodynamics (Mahrt, 1998; Holtslag *et al.*, 2013; Zardi and Whiteman, 2013; Steeneveld, 2014). Moreover, to meet the requirements of the extremely cold and demanding conditions that characterise the Antarctic Peninsula (and Antarctica in general), polar-optimised versions of some atmospheric models such as the Weather Research and Forecasting (WRF: Turton *et al.*, 2017), MAR (Modèle Atmosphérique Régionale: Datta *et al.*, 2019), RACMO2 (Regional Atmospheric Climate Model: van Wessem *et al.*, 2016), and the Consortium for Small-Scaled Modelling (COSMO) model in Climate Mode (CCLM: Zentek and Heinemann, 2020) have been developed. By comparison, the kilometre-scale limited-area configuration of the UK Met Office Unified Model (MetUM) numerical weather prediction system has been used to conduct many studies of the Antarctic Peninsula despite having little or no polar-optimisation (e.g. Orr *et al.*, 2004; 2008; 2015; Luckman *et al.*, 2014; Elvidge *et al.*, 2015; 2016; 2020; King *et al.*, 2015; Kuipers Munneke *et al.*, 2018; Dell *et al.*, 2020; Gilbert *et al.*, 2020; 2021; Mottram *et al.*, 2021). However, although the MetUM is not polar-optimised, its non-hydrostatic core enables it to be run at higher scales (sub-kilometre) than either MAR or RACMO2, which both use a hydrostatic core and are limited to a minimum grid spacing of 5–10 km (van Wessem *et al.*, 2016; Datta *et al.*, 2019).

Elvidge *et al.* (2015; 2020) and Grosvenor *et al.* (2014) suggest that a grid spacing of 1.5 km gives a reasonably accurate representation of foehn conditions over the LCIS (compared to aircraft and surface observations). A grid spacing of around 5 km is employed for longer (multi-year) simulations due to the lower computational cost (e.g. Datta *et al.*, 2019; Kirchgaessner *et al.*, 2019; Turton *et al.*, 2020; Gilbert *et al.*, 2021). However, there is evidence that the model results/performance can be sensitive to resolution in the 5 to 1.5 km range, raising concerns that a grid spacing of 5 km is not adequate (e.g. Elvidge *et al.*, 2015; Turton *et al.*, 2017). Moreover, our understanding of the added benefit of sub-kilometre scale grid spacing, such as whether model convergence occurs at finer resolutions (and thus better-resolved orography) and whether the realism of foehn events is generally improved, is non-existent due to the absence of such simulations in this region (Knist *et al.*, 2020). Further work is also required to clarify the interaction between foehn and cold-air pools over the LCIS, as well as their representation in atmospheric models, as this has been shown to play a crucial role in controlling the near-surface temperature in other regions (Flamant *et al.*, 2006; Haid *et al.*, 2020).

The aim of this study is to address some of these deficiencies by examining the main biases in a MetUM simulation of the LCIS at kilometre scale (4 km grid spacing) for a one-month period during January/February 2011. This is followed by a case-study examination of the impact of different kilometre and sub-kilometre scale grid spacing (by comparing 4, 1.5 and 0.5 km grid spacing) on the simulation of a foehn event that occurred on 27 January 2011, which encountered an existing cold-air pool. The foehn event was in response to a ridge of high pressure to the west of the Antarctic Peninsula on 26 January (resulting in southeasterly cross-barrier flow), which gradually migrated south during 27 January. This resulted in a west-to-east flow of around 4 $m \cdot s^{-1}$ incident to the Antarctic Peninsula and a non-dimensional mountain height of $\widehat{h} \sim 4$, that is, characterised by a highly nonlinear flow regime. We refer to Elvidge *et al.* (2015) for further details, which previously examined this case-study.

2 | MODELS, OBSERVATIONS AND METHODS

2.1 | MetUM forecast model

The atmospheric model used is the kilometre-scale limited-area configuration of version 11.1 of the MetUM numerical weather prediction system. This uses the ENDGame (Even Newer Dynamics for General atmospheric modelling of the environment) dynamical core and a rotated pole to ensure a rectangular, regular latitude–longitude grid. ENDGame uses a mass-conserving semi-implicit semi-Lagrangian numerical scheme to solve the discretised equations of motion for

a non-hydrostatic, fully compressible, deep atmosphere (Wood *et al.*, 2014; Walters *et al.*, 2017). The model uses the Regional Atmosphere physics configuration for mid-latitudes (RA1M), described by Bush *et al.* (2020). As its name suggests, the RA1M configuration has been primarily developed to optimise model performance over the midlatitudes (Bush *et al.*, 2020).

The RA1M package includes parametrization schemes for cloud microphysics and the atmospheric boundary layer, which have both been identified as being particularly important for simulating the near-surface meteorological conditions over the LCIS (King *et al.*, 2015; Gilbert *et al.*, 2020; 2021). The cloud microphysics is a single-moment scheme (Wilson and Ballard, 1999), but the version used here has extensive modifications described by Gilbert *et al.* (2020; 2021) to improve the representation of cloud phase over the LCIS. These modifications considerably improved the simulation of downwelling short-wave and long-wave radiation at the surface, and therefore the surface energy budget. The atmospheric boundary-layer parametrization uses a "blended" approach (Bush *et al.*, 2020), which transitions from a one-dimensional (1-D) vertical turbulent mixing scheme at relatively coarse horizontal resolutions ranging from a few kilometres to tens of kilometres (i.e. turbulent length-scales less than the grid scale) to a 3-D Smagorinsky turbulent mixing scheme at finer horizontal resolutions ranging from a few kilometres to hundreds of metres (i.e. turbulent length-scales comparable to the grid scale). For stable boundary layers, the scheme uses the "sharp" stability function (Brown *et al.*, 2008). Additionally, the JULES (Joint UK Land Environment Simulator) land surface model is used (Walters *et al.*, 2019). This includes the option of a simple composite snow/soil layer (or "zero-layer" snow scheme), which was employed here (Best *et al.*, 2011).

The three nested model domains at horizontal resolutions of 4, 1.5 and 0.5 km are shown in Figure 1. The dynamical time step employed is 20 s for the 4 and 1.5 km models and 12 s for the 0.5 km model, which are small enough to avoid instability and satisfy the Courant–Friedrichs–Lewy (CFL) criterion (Kalnay, 2002). An additional impact of the short time steps (and the ENDGame dynamical core) is a reduction in damping of gravity-wave motion, resulting in an improved simulation of mountain waves (Shutts and Vosper, 2011; Walters *et al.*, 2017). Note that, apart from the changes to the cloud scheme, the physics configuration of the 4 and 1.5 km models used here are more or less the same as the UK 4 and 1.5 km variable resolution models (UKV) developed by the Met Office to provide weather forecasts for the United Kingdom and Europe (Tang *et al.*, 2013), that is, these versions of the model used here are largely developed

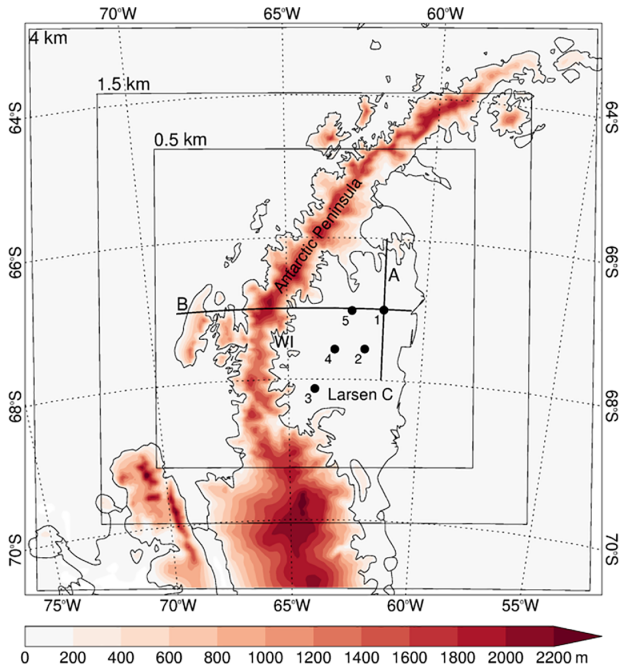

FIGURE 1 Map showing the MetUM nested limited-area domains over the Antarctic Peninsula and Larsen C Ice Shelf at horizontal resolutions of 4, 1.5 and 0.5 km (marked by the square boxes). Also shown is the orography (shading) of the model at a horizontal resolution of 4 km, as well as the coastline and ice shelf extent (black lines). The positions of AWS1, 2, 3, 4 and 5 are shown as the filled black circles (and labelled 1, 2, 3, 4 and 5, respectively). The thick lines labelled "A" and "B" indicate the north–south and west–east vertical transects examined in Figures 6 and 7, respectively, which pass through the AWS1 site. The location of Whirlwind Inlet is labelled "WI", which is shown in detail in Figure 8 [Colour figure can be viewed at wileyonlinelibrary.com]

and tuned for the midlatitudes. By contrast, the experiments using the 0.5 km model are highly novel – although Alexander *et al.* (2017) used MetUM simulations at 0.5 and 0.1 km grid spacing to investigate the formation of small-scale orographic gravity waves forced by coastal topography along the East Antarctic coastline.

The outer 4 km model domain covers the Antarctic Peninsula and the LCIS (domain size of 220×220 grid points), while the two additional (one-way nested) 1.5 and 0.5 km model domains cover the northern Antarctic Peninsula and LCIS (domain size of 450×450 and $1{,}000 \times 1{,}000$ grid points, respectively). Boundary conditions for the 1.5 km (0.5 km) model are derived from the 4 km (1.5 km) model. All three models employ 70 vertical levels (going up to 40 km), which are terrain-following near the surface and constant height at upper levels. The lowest 1,000 m part of the atmosphere contains 16 vertical levels, which are arranged at 5, 22, 45, 75, 112, 155, 204, 261, 324, 394, 470, 553, 643, 739, 842 and 951 m above the surface. The finer vertical resolution nearer the surface is

important for good representation of the turbulent vertical exchange processes in the boundary layer.

The orography used by the 4, 1.5 and 0.5 km models is derived from the high-resolution (200 m) Radarsat Antarctic Modelling Project (RAMP) digital elevation model (Liu *et al.*, 2015). Due to the very steep terrain, some smoothing of the 4 and 1.5 km (0.5 km) orography was required, which was generated by convolution using a normalised 2-D Gaussian kernel with a standard deviation of 0.6 grid points (0.8485 grid points). The coastline and ice shelf extent are taken from the Scientific Committee on Antarctic Research (SCAR) Antarctic Digital Database.

The 4 km model is nested within a 12 km version of the model (domain size of 150×150 grid points), which has a much larger limited-area domain encompassing the whole of the Antarctic Peninsula and the surrounding ocean (not shown). Initial and boundary conditions for the 12 km model are provided by the global model configuration of the MetUM at N320 resolution (640×480 grid points, equivalent to a horizontal resolution of ~40 km at midlatitudes), which is initialised by ERA-Interim reanalysis (Dee *et al.*, 2011).

2.2 | Observations

Measurements of pressure, air temperature, wind speed and wind direction from five Automatic Weather Stations (AWSs) distributed across the LCIS were utilised. The location of the five sites is shown in Figure 1 and they are hereafter referred to as AWS1, 2, 3, 4 and 5. Also used are measurements of incoming and outgoing short-wave radiation and incoming and outgoing long-wave radiation from AWS1. AWS1 and 2 are owned by the Institute for Marine and Atmospheric Research (IMAU), Utrecht University, and are described by Kuipers Munneke *et al.* (2012) and Jakobs *et al.* (2020). AWS3, 4 and 5 were owned by the Cooperative Institute for Research in Environmental Sciences (CIRES), University of Colorado, and are described by Kuipers Munneke *et al.* (2018). The stations have a mast height of 3–4 m, although this height is variable with time due to snow accumulation, with the instrument measuring wind speed and direction situated on the top of the mast. The temperature sensors are naturally ventilated and located at a standard screen-level height of >1.5 m. Following Smeets *et al.* (2018), warm-biased temperature measurements from AWS1 and 2 due to weak wind conditions causing low ventilation rates when incoming solar radiation is high were corrected (see also Kuipers Munneke *et al.*, 2012).

Also used are radiosonde measurements from the location of AWS1 at 1200 and 1800 UTC on 27 January 2011, which were part of the month-long Orographic Flows and the Climate of the Antarctic Peninsula (OFCAP) field campaign (Kirchgaessner *et al.*, 2014). These launches coincided with the occurrence of the foehn event over the LCIS examined in this study. Cloud data from the Moderate Resolution Imaging Spectroradiometer (MODIS) based on corrected reflectance images from the Terra overpass at 1309 UTC on 27 January 2011 are also employed (Platnick *et al.*, 2015), which again also coincides with the foehn event.

2.3 | Experimental methodology

The MetUM 4 km model was run twice daily at 0000 and 1200 UTC from 8 January 2011 to 8 February 2011 for 24 hr, with output saved at T + 15, T + 18, T + 21 and T + 24 hr. Earlier output was discarded as spin-up. King *et al.* (2015) showed that this period, which coincided with the OFCAP field campaign, was broadly representative of typical summer conditions over the LCIS. The saved output was used to create a continuous time series of instantaneous 3-hourly model values of surface pressure, 10 m zonal wind speed, 10 m meridional wind speed, 1.5 m air temperature, and 1.5 m specific humidity at each of the locations of the five AWS sites from 1500 UTC on 8 January 2011 to 0000 UTC on 9 February 2011. These model data were subsequently compared with the corresponding time series of measurements at 3-hourly intervals, derived from the AWS data. To compare with the model 10 m wind speed, the observed wind speed was adjusted to a height of 10 m by assuming a logarithmic wind profile and a surface roughness length of 1.0×10^{-4} m, which is typical of snow over land (Beljaars and Holtslag, 1991). The measured relative humidity at low temperature was corrected using the method of Anderson (1994) prior to transforming it to specific humidity for direct comparison with model output.

The computationally expensive MetUM 1.5 and 0.5 km models were only run to obtain output coinciding with the case-study foehn event on 27 January 2011. Two model runs were initialised at 1200 UTC on 26 January and 0000 UTC on 27 January and ran for 24 hr, with output saved at an earlier forecast time of T + 12 hr, as well as T + 15, T + 18, T + 21 and T + 24 hr. Earlier output was discarded as spin-up. This resulted in a series of 3-hourly model outputs from 0000 to 2400 UTC for 27 January at both 1.5 and 0.5 km grid spacing. Analogous runs using the MetUM 4 km model were also completed to obtain corresponding output for 27 January at 4 km grid spacing, enabling the performance of the three models to be compared. The output from these runs included the instantaneous surface radiation components (i.e. incoming and outgoing surface short-wave and long-wave radiation) and 1.5 m temperatures, which are compared with the measured values.

Instantaneous values of potential temperature and wind speed on vertical levels were also saved, and are extracted for the location of AWS1 to compare them with measurements from the coinciding radiosonde launches. Additionally, the instantaneous values of low-level (as well as mid- and high-level) cloud fraction were saved, which are compared with the MODIS cloud imagery.

As foehn events over the LCIS can sometimes exhibit high spatial and temporal variability (Cape *et al.*, 2015), hourly averaged values of potential temperature and wind speed on vertical levels from the 4, 1.5 and 0.5 km models were further saved for 27 January. Also saved were hourly averaged values of 1.5 m temperature, 10 m zonal wind speed, and 10 m meridional wind speed. By averaging temporally, the high-frequency variations that occur in the instantaneous output will be reduced, making the agreement/disagreement between the models clearer. Additionally, hourly accumulated values of the temperature tendency from both the dynamics and the total physics contribution were saved, and again extracted for the location of AWS1. Hourly accumulated values were used as the instantaneous temperature tendencies can be relatively noisy. However, to verify the robustness of the hourly accumulated values, analogous results based on six-hourly accumulated values of the temperature tendency were also saved. The dynamical temperature tendency represents the contribution from horizontal and vertical advection, while the total physics temperature tendency includes contributions from the physics schemes employed by the model, such as vertical turbulent transport within the boundary-layer scheme, diffusion, and radiative fluxes.

Following Orr *et al.* (2014), a further sensitivity experiment was conducted for 27 January using the MetUM 4 km model but replacing the "sharp" stability function with the "long-tail" stability function for the boundary-layer scheme, to examine the impact of stronger turbulent mixing for statically stable conditions (Brown *et al.*, 208).

3 | RESULTS

The results section comprises a first part that looks at the model performance over the LCIS for the one-month period at 4 km grid spacing, followed by a second part that focuses on the foehn case-study and its interaction with a cold-air pool at 4, 1.5 and 0.5 km grid spacing.

3.1 | Evaluation of 4 km model performance for a one-month period

Figure 2 compares the 3-hourly measurements at AWS1 with the corresponding 4 km output for the period from 1500 UTC on 8 January 2011 to 0000 UTC on 9 February 2011. Kuipers Munneke *et al.* (2012) suggest that this location (and also the locations of AWS2, 3, 4 and 5) is typical of the flat and homogeneous snow surface that characterises the LCIS. The measured pressure at AWS1 is dominated by synoptic variations, which are accurately captured by the MetUM (Figure 2a).

The measured air temperature at AWS1 is dominated by a pronounced diurnal temperature cycle, which the 4 km model struggles to realistically capture (Figure 2b). Its representation of the night-time minimum temperature is especially problematic and includes nights with both excessively low temperatures (by over 5 °C, such as on 9 and 27 January 2011) and high temperatures (such as on 30 and 31 January and 4 February 2011). The model is better able to represent the daytime maximum temperature (such as on 19 to 23 January 2011) but struggles to simulate daytime air temperatures above freezing on the few occasions when this was observed (such as on 17 and 18 January 2011). Note that it is unlikely that such biases are due to measurement errors during occasions of excessively high incoming solar radiation because of low wind speed, as this has been corrected for (Kuipers Munneke *et al.*, 2012). The measured specific humidity at AWS1 also shows a diurnal cycle (Figure 2e). Due to the strong correlation between specific humidity and temperature, many of the errors in the 4 km model are coincident with errors in temperature.

The measured wind speed at AWS1 shows a strong influence of synoptic forcing (such as from 9 to 13 January and 3 to 7 February 2011) during which speeds reached 15 $m \cdot s^{-1}$ (Figure 2c). Both the strengthening and subsequent weakening of the winds during these events are captured well by the 4 km model (as also found by Orr *et al.*, 2014). The diurnal variation in model wind speed is also broadly in agreement with the measurements, with the maximum daily wind speeds occurring at approximately the same time as the maximum daytime temperatures, suggesting that the wind behaviour is influenced by increased mixing (due to the reduction in near-surface stability as the boundary layer heats up) transporting higher momentum air from aloft downwards to the near-surface.

The representation of wind direction at AWS1 by the model (Figure 2d) is reasonable when the wind direction is persistent and the wind speed is reasonably strong (such as from 4 to 7 February 2011), but poor when the wind direction is noticeably varying (although this is often also associated with weak winds, such as on 14, 17 and 26 January 2011).

Table 1 shows the corresponding error statistics for the 4 km model for the period 8 January to 9 February 2011 for AWS1, as well as the other four sites (AWS2, 3, 4 and 5), demonstrating that the 4 km model performance

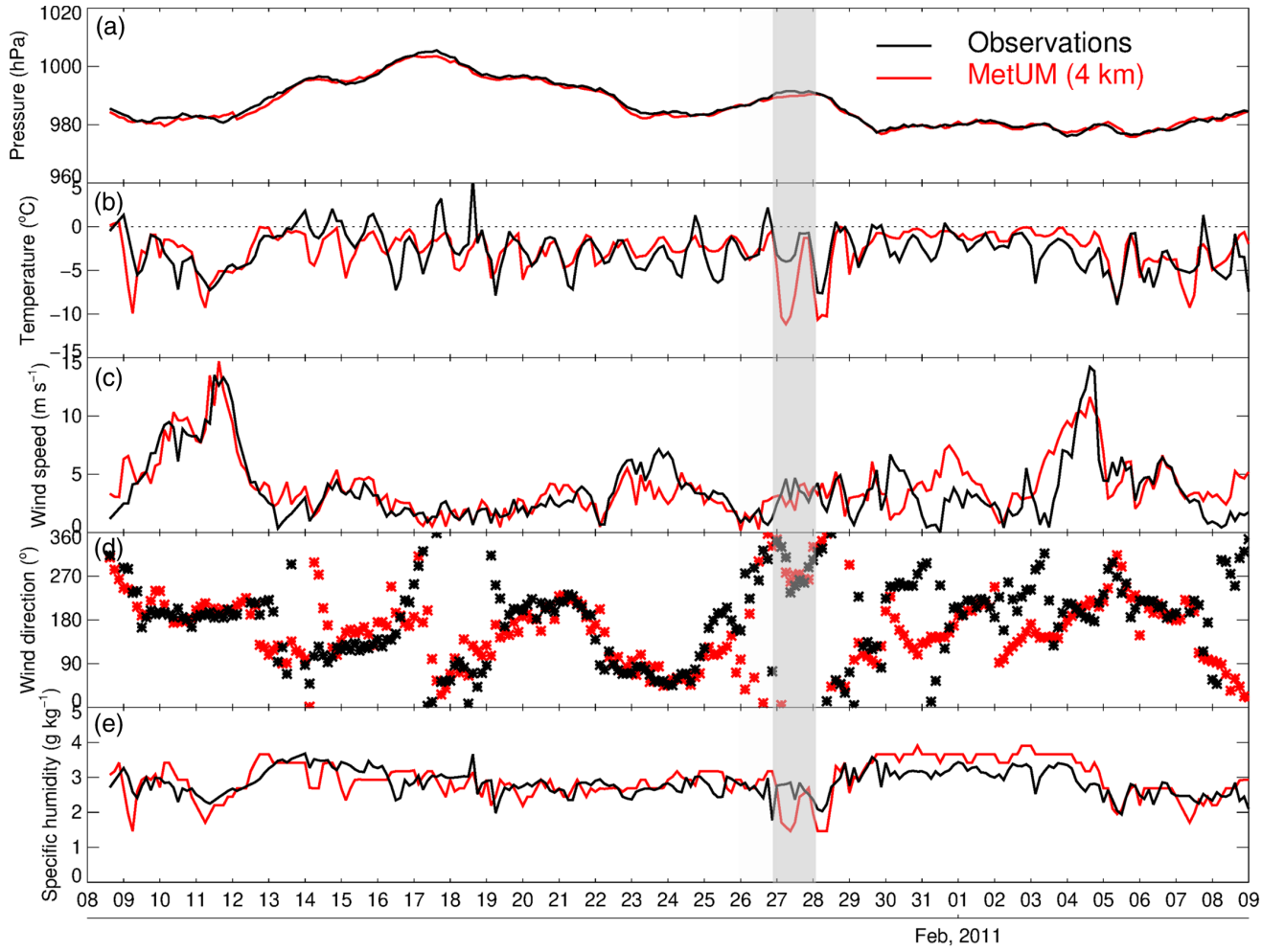

FIGURE 2 Comparison of the time-series of 3-hourly measurements (black) and MetUM output (red) at a horizontal resolution of 4 km at the AWS1 site for (a) pressure (hPa), (b) temperature (°C), (c) wind speed ($m \cdot s^{-1}$), (d) wind direction (°) and (e) specific humidity ($g \cdot kg^{-1}$), from 1500 UTC on 8 January 2011 to 0000 UTC on 9 February 2011. The foehn wind case-study on 27 January 2011 is highlighted by the semi-transparent vertical grey bar [Colour figure can be viewed at wileyonlinelibrary.com]

TABLE 1 Statistical evaluation of MetUM output at a horizontal resolution of 4 km for surface pressure, 1.5 m temperature, 10 m wind speed and 1.5 m specific humidity, at the five AWS sites for the period from 1500 UTC on 8 January 2011 to 0000 UTC on 9 February 2011

	Pressure			Temperature			Wind speed			Specific humidity		
Site	Bias (hPa)	RMSE (hPa)	Corr.	Bias (°C)	RMSE (°C)	Corr.	BIAS ($m \cdot s^{-1}$)	RMSE ($m \cdot s^{-1}$)	Corr.	BIAS ($g \cdot kg^{-1}$)	RMSE ($g \cdot kg^{-1}$)	Corr.
AWS1	−0.44	0.99	0.99	0.08	2.19	0.53	0.36	1.87	0.76	−0.01	0.38	0.95
AWS2	−0.78	1.29	0.99	−0.36	1.81	0.71	−0.06	1.70	0.83	−0.04	0.37	0.95
AWS3	−0.57	1.02	0.99	−0.02	2.07	0.60	−0.08	1.80	0.80	−0.03	0.38	0.95
AWS4	0.99	1.30	0.99	0.06	1.96	0.60	−0.06	1.70	0.74	−0.06	0.45	0.93
AWS5	0.07	0.90	0.99	−0.11	2.11	0.59	0.02	1.73	0.77	0.15	0.43	0.95

Note: Statistics used are bias (model minus measured value), root-mean-square-error (RMSE), and correlation coefficient.

at AWS1 in terms of pressure, temperature, wind speed and specific humidity is largely similar across all LCIS stations. One noteworthy difference is that the correlation coefficients for temperature and wind speed are higher at AWS2 than at AWS1, suggesting improved model performance at AWS2.

3.2 | Simulation of foehn event at 4, 1.5 and 0.5 km grid spacings

The largest temperature errors of the month-long MetUM 4 km simulations at AWS1 occur on 27 January (Figure 2b), that is, coinciding with the foehn event that occurred at this time. For example, at around 0900 UTC (0600 local time, LT) on 27 January the simulated nocturnal minimum temperature was around 8 °C too low (Figure 2b). Similarly sized nocturnal cold biases are also apparent at AWS2, 3, 4 and 5 in the 4 km model simulation on 27 January (Figure 3), suggesting that the error is widespread over the LCIS. The remaining results will focus on this foehn event, and especially whether we see an improvement in the model results as the horizontal resolution is increased from 4 km to 1.5 and 0.5 km.

Figure 3 also includes results from the MetUM at 1.5 and 0.5 km resolution on 27 January. In general, although there is some reduction in the cold bias in the 0.5 km model compared to the 4 km model (e.g. at AWS1 and 2), there is no systematic evidence of convergence of the model temperature value towards the measured values with increasing horizontal resolution.

At 1200 UTC (0900 LT) on 27 January (i.e. 3 hr after the large cold bias occurred) the radiosonde profile of potential temperature at AWS1 shows a strong inversion between the surface and around 200 m above the surface, consistent with the formation of a ground-based cold-air pool (Figure 4a). Above this feature the atmospheric conditions are near-neutral well-mixed (Figure 4a). The radiosonde profile at 1200 UTC also shows a relatively weak low-level wind jet, which has a maximum speed of around 8 $m \cdot s^{-1}$ at a height of ~300 m (Figure 4c). The radiosonde profile at 1800 UTC (1500 LT) on 27 January shows that both the cold-air pool and low-level wind jet have largely disappeared and the atmospheric conditions are near-neutral throughout the lower atmosphere, with the exception of a region between around 100 and 200 m above the surface (Figure 4b,d).

Compared to the observations, the MetUM 4 km profile of potential temperature at 1200 UTC (based on instantaneous output) is too cold near the surface and throughout the lower atmosphere (by around 2 K), and erroneously simulates a shallow near-neutral layer between the surface and ~50 m (Figure 4a). Above this, the simulation shows a shallow region of highly stable air capping the ground-based near-neutral layer and the formation of a wind jet (Figure 4c). Although both these features are broadly in agreement with the observations, the strength of both the stable layer and wind jet are anomalously strong. At 1200 UTC the profiles of potential temperature and wind speed simulated by the 1.5 and 0.5 km models are largely in agreement with the 4 km model. However,

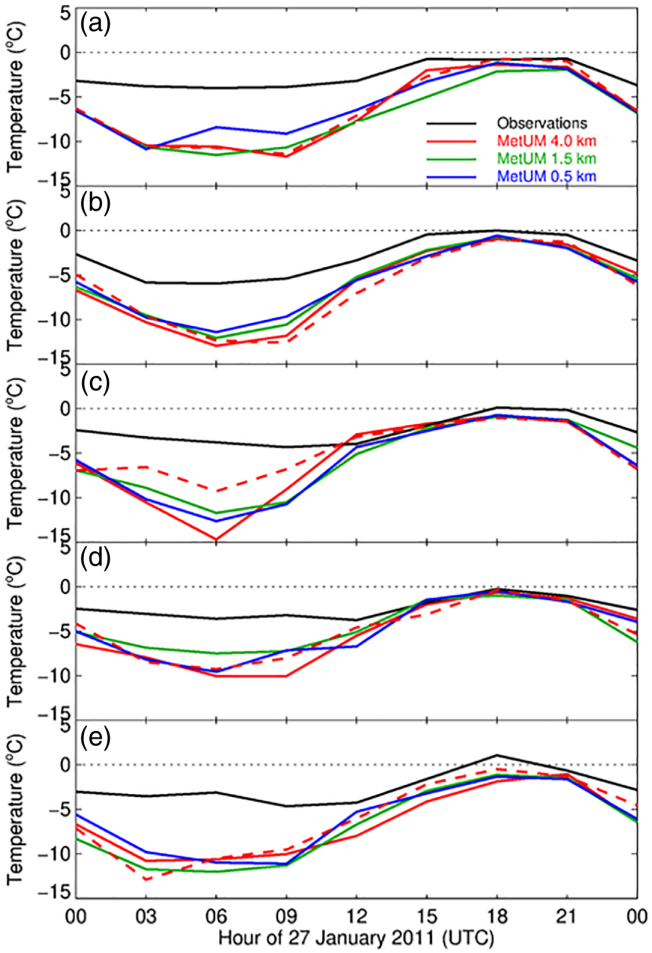

FIGURE 3 Comparison of the time-series of 3-hourly temperature measurements (black) and MetUM 1.5 m temperature (°C) output at horizontal resolutions of 4 km (red), 1.5 km (green) and 0.5 km (blue), during the foehn wind case-study from 0000 to 2400 UTC on 27 January 2011 at (a) AWS1, (b) AWS2, (c) AWS3, (d) AWS4 and (e) AWS5. The dashed red line shows results for the MetUM 4 km simulation with the "long-tail" stability function for stable conditions. The MetUM results are based on the combination of instantaneous output from runs initialised at 1200 UTC on 26 January 2011 (contributing fields at T + 12, T + 15, T + 18, T + 21 and T + 24 hr) and 0000 UTC on 27 January 2011 (contributing fields at T + 15, T + 18, T + 21 and T + 24 hr) [Colour figure can be viewed at wileyonlinelibrary.com]

discrepancies between the models are evident in their representation of the surface-based near-neutral layer and the strength of the low-level jet. By contrast, at 1800 UTC the simulated potential temperature profile in the 4, 1.5 and 0.5 km models are in relatively good agreement with the observations.

In the absence of radiosonde measurements from any other location apart from AWS1 and to better understand the atmospheric conditions over the entire ice shelf, Figure S1 shows simulated profiles of potential temperature and wind speed at 1200 UTC for all five AWS

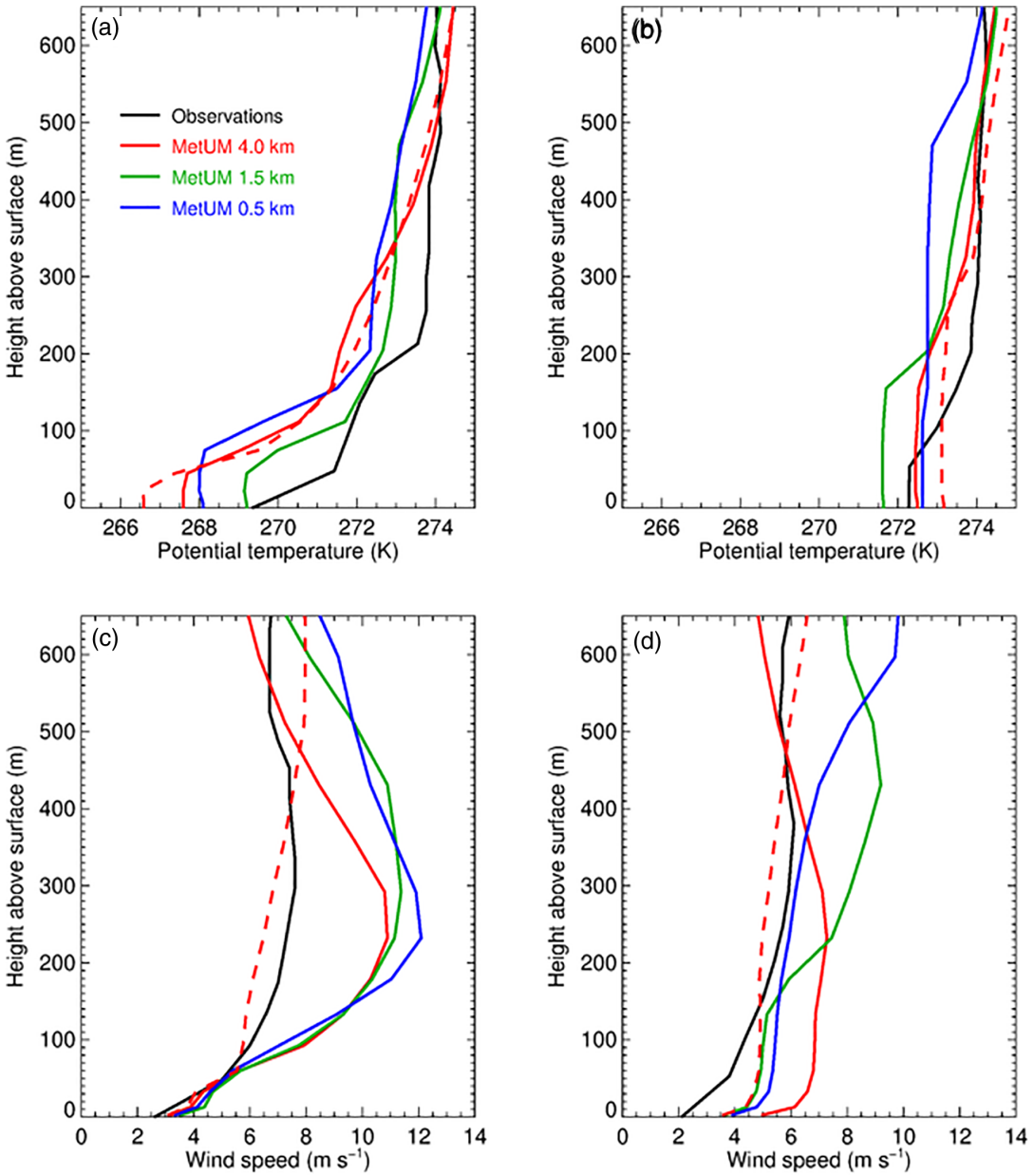

FIGURE 4 Comparison of the vertical profile of measured (black) and MetUM simulated (a,b) potential temperature (K) and (c,d) wind speed (m·s^{-1}), at horizontal resolutions of 4 km (red), 1.5 km (green) and 0.5 km (blue), during the foehn wind case-study at (a,c) 1200 UTC (0900 LT) on 27 January 2011 and (b,d) 1800 UTC (1500 LT) on 27 January 2011. The profiles are over the AWS1 site (see Figure 1 for location). The dashed red line shows results for the MetUM 4 km simulation with the "long-tail" stability function for stable conditions. The MetUM results are based on instantaneous output saved at T + 12 and T + 18 hr from a run initialised at 0000 UTC on 27 January 2011 [Colour figure can be viewed at wileyonlinelibrary.com]

sites based on hourly averaged values for the 4, 1.5 and 0.5 km models. The simulated profiles at AWS2, 3, 4 and 5 are broadly similar to AWS1, with the potential temperature profile characterised by a strongly stable layer near the surface and a less stable layer/near-neutral conditions at upper levels. However, only AWS5 is characterised by a ground-based near-neutral layer, which may be erroneously simulated if guidance is taken from the AWS1 results. The simulated wind profile at each of the locations shows a distinct low-level jet at a height of between 200 and 300 m, with maximum speeds reaching 15 m·s^{-1}. However, it is noticeable that the disagreement between models is much larger at AWS2, 3, 4 and 5 than at AWS1. For example, sites such as AWS3, 4 and 5 are characterised by differences of up to 5 m·s^{-1} in the magnitude of the peak wind speed at the different resolutions. By 1800 UTC, the simulated atmospheric conditions are largely near-neutral throughout the lower atmosphere at

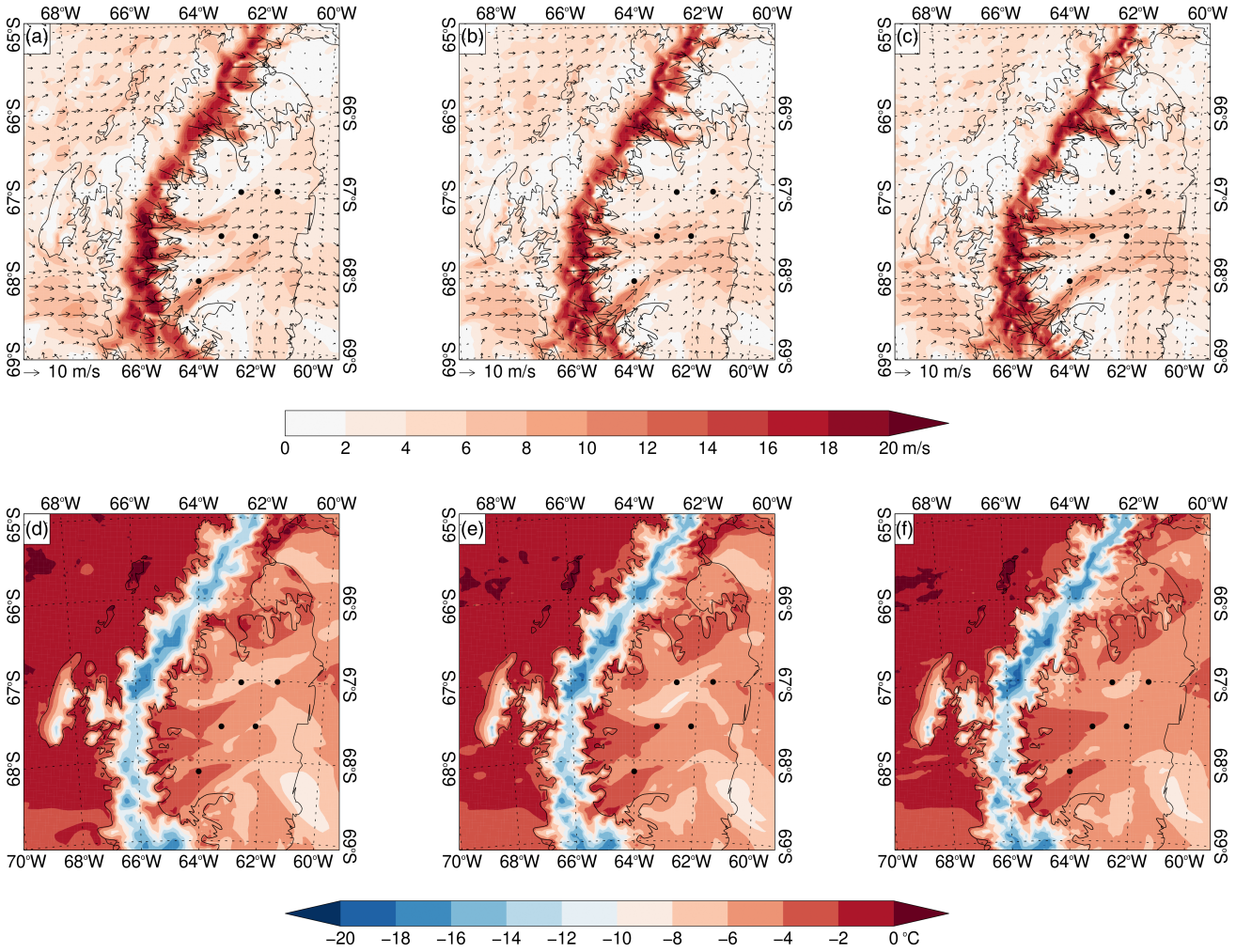

FIGURE 5 Comparison of the MetUM simulated (a–c) hourly-averaged 10 m wind speed ($m \cdot s^{-1}$, contours) and vectors ($m \cdot s^{-1}$, arrows), and (d–f) hourly averaged 1.5 m temperature (°C, contours), during the foehn wind case-study at 1200 UTC (0900 LT) on 27 January 2011 over the northern Antarctic Peninsula and LCIS at horizontal resolutions of (a,d) 4 km, (b,e) 1.5 km and (c,f) 0.5 km. The locations of the five AWS sites are displayed as filled black circles (also shown in Figure 1). The length of the arrows relates to the wind speed. Note that for comparison purposes the 1.5 and 0.5 km model output (for both wind speed and temperature) are re-gridded onto the 4 km model grid, and only every 5th wind arrow is shown. The MetUM results are based on hourly averaged output saved at T + 12 hr from a run initialised at 0000 UTC on 27 January 2011 [Colour figure can be viewed at wileyonlinelibrary.com]

all the AWS sites, and the low-level wind jets have largely disappeared (Figure S2). However, considerable disagreement in the model representation of the wind speed profile still occurs.

The observed erosion of the cold-air pool and the substantial change in the temperature structure between 1200 and 1800 UTC at AWS1 (Figure 4) could be caused by either daytime heating from below or by downward mixing of the moderately strong winds associated with the low-level jet, or by a combination of both. Although we recognise that this feature is poorly represented by the MetUM, we will still use the model to investigate the spatial patterns further. Figure 5 shows the hourly averaged simulated 10 m wind speed and 1.5 m temperature at 1200 UTC on 27 January 2011 for the 4, 1.5 and 0.5 km models. This shows distinct narrow foehn jets emanating from various inlets onto the LCIS. The foehn jets have speeds of 5–10 $m \cdot s^{-1}$ (and even higher close to the inlets) as the air travels eastwards over the LCIS. The jets reach as far as the eastern margins of the LCIS, albeit weaker and cooler compared to close to the inlets. Foehn jets are apparent at the locations of all the AWS sites, suggesting that they could thus be responsible for the low-level jets apparent in the wind speed profiles (Figures 4 and S1) and therefore playing a role in the erosion of the cold-air pool by downward mixing of their moderately strong winds. This is likely to occur in combination with daytime heating from below due to the increase in insolation from 1200 UTC (0900 LT) to 1800 UTC (1500 LT).

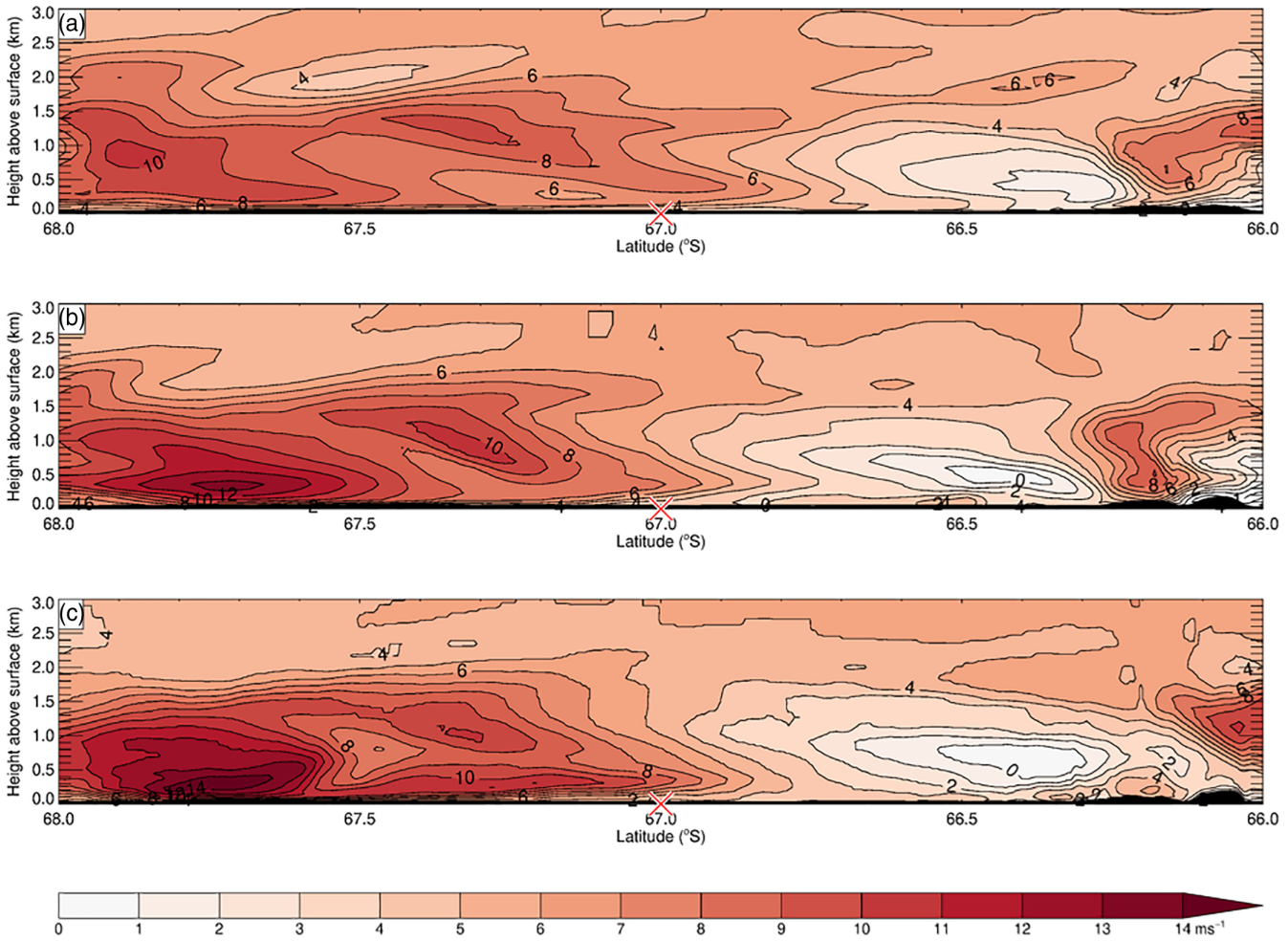

FIGURE 6 Vertical cross-sections of the MetUM simulated hourly-averaged westerly wind speed ($m \cdot s^{-1}$, contours) along transect "A" in Figure 1 during the foehn wind case-study at 1200 UTC (0900 LT) on 27 January 2011 at horizontal resolutions of (a) 4 km, (b) 1.5 km and (c) 0.5 km. The cross-section runs from south to north (from 68° to 66°S) along longitude 61.50°W and cuts through the location of AWS1, which is marked by the red cross in the panels (and located at 67.01°S, 61.50°W). The MetUM results are based on hourly averaged output saved at T + 12 hr from a run initialised at 0000 UTC on 27 January 2011 [Colour figure can be viewed at wileyonlinelibrary.com]

Across the LCIS, both the simulated speed and direction of the foehn jets varies with horizontal resolution, with no apparent convergence in the results to increasing resolution. These differences are especially evident for the jets emanating from Whirlwind Inlet (labelled "WI" in Figure 1). The foehn jet emanating from Whirlwind Inlet particularly affects AWS4. At this location, both the 10 m wind speed (Figure 5) and wind speed profile (Figure S1h) show considerable disagreement between the different horizontal resolutions. The anomalously high 1.5 m temperatures that are associated with the foehn jets also vary by ~2 °C between the different model resolutions (Figure 5). By contrast, upstream of the Antarctic Peninsula the results are similar for all resolutions. Large differences in the spatial structure of the simulated foehn jets in the lower 2 km of the atmosphere between different horizontal resolutions are even more apparent in Figure 6, which shows a south–north vertical cross-section of the hourly averaged westerly winds over the eastern sector of the LCIS (labelled line "A" in Figure 1, which also passes through the location of AWS1) at 1200 UTC on 27 January. This confirms that the height of the foehn jets (i.e. the height of the maximum wind speed) occurs at around 300 m above the surface.

To examine whether this lack of resolution dependence/convergence at 1200 UTC on 27 January at sub-kilometre scale is also apparent in the MetUM representation of features common to foehn events such as upstream low-level blocking, downslope winds, upper-level wave breaking, and leeside hydraulic jumps, Figure 7 shows a west–east vertical cross-section of the simulated hourly averages of potential temperature over the northern sector of the LCIS at this time (labelled line "B" in Figure 1, which passes through the location of AWS1). This shows that these features appear largely similar at 4 and 1.5 km. By contrast, the 0.5 km

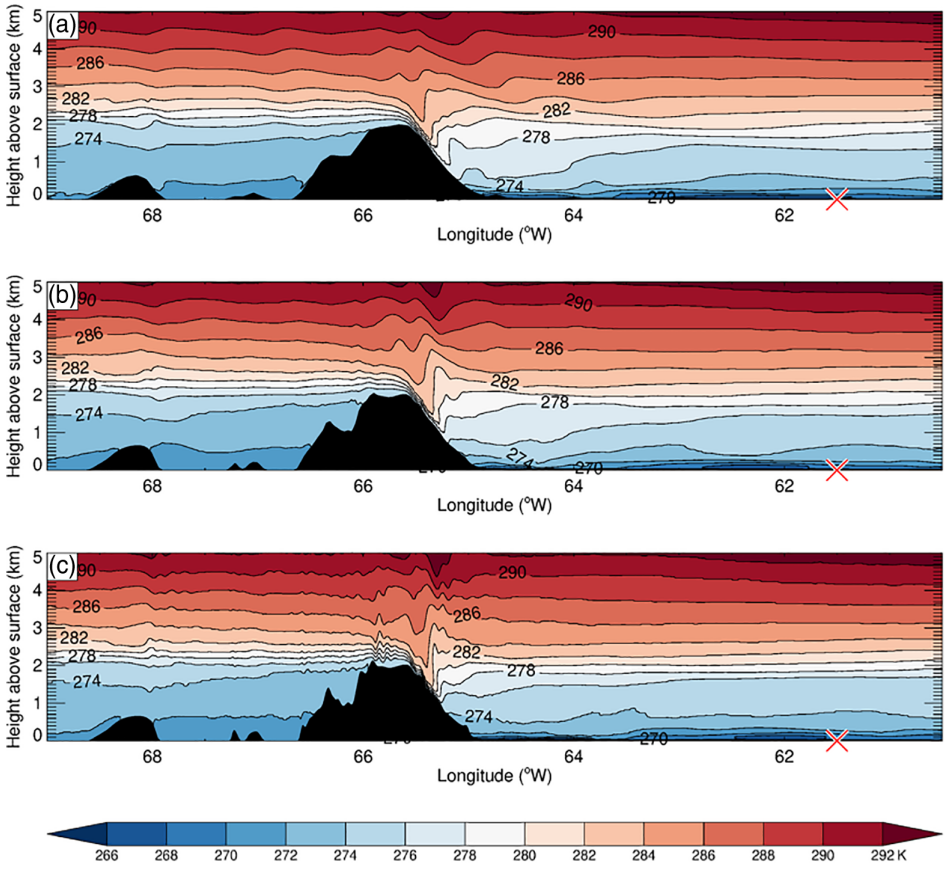

FIGURE 7 Vertical cross-sections of the MetUM simulated hourly-averaged potential temperature (K, contours) along transect "B" in Figure 1 during the foehn wind case-study at 1200 UTC (0900 LT) on 27 January 2011 at horizontal resolutions of (a) 4 km, (b) 1.5 km and (c) 0.5 km. The cross-section runs from west to east (from 69° to 60.5°W) at latitude 67.01°S and cuts through the location of AWS1, which is marked by the red cross in the panels (and located at 67.01°S, 61.5°W). The case-study is associated with west-to-east flow across the Antarctic Peninsula, so in the panels the wind is blowing from left to right. The MetUM results are based on hourly averaged output saved at T + 12 hr from a run initialised at 0000 UTC on 27 January 2011 [Colour figure can be viewed at wileyonlinelibrary.com]

simulation shows a sharper hydraulic jump developing quite high up the leeside slope (as well as a layer of strong stability at around 2 km above the surface on the lee side) compared to the 4 and 1.5 km results. The leeside warming in all models is local to the Antarctic Peninsula topography, that is, it does not extend a considerable distance across the LCIS. Differences in the vertical temperature structure between the 4, 1.5 and 0.5 km models are apparent at low-level (<0.5 km) at the site of AWS1 and its surroundings, although these are not as large as the differences found at the foot of the Peninsula's eastern slopes under foehn conditions (Kirchgaessner *et al.*, 2019).

4 | DISCUSSION

The differences in the representation of the foehn jets for the three horizontal model resolutions suggest that the models have difficulties capturing this phenomenon realistically (Figures 4–6 and S1). Both the dynamics of the jets and their interaction with an existing cold-air pool are poorly captured (Figures 4 and S1). It suggests that the models fail to capture the vertical mixing in the boundary layer and its impact on thermodynamics realistically under these conditions, through the model-resolved dynamics and/or the sub-grid turbulent mixing (Mahrt, 1998; Tastula and Vihma, 2011; Holtslag *et al.*, 2013; Zardi and Whiteman, 2013; Steeneveld, 2014). Additionally, it is worth pointing out that the stable boundary-layer regime in general (and not just cold-air pools) can be associated with the development of low-level wind jets, such as in response to diurnal variations in surface heating and Coriolis effects (Blackadar, 1957; Thorpe and Guymer, 1977; Owinoh *et al.*, 2005).

To better understand why we see this behaviour, Figure 8 compares the model orography at 4, 1.5 and 0.5 km for the region including Whirlwind Inlet, which was a notable source of low-level wind jets for the case-study. The model orography at 1.5 and 0.5 km appears to have largely converged (i.e. only small differences exist between them). However, despite this we do not see any convergence in the foehn jets at 1.5 and 0.5 km (Figure 5). By contrast, the upwind conditions, which govern the mountain flow regime during the foehn event, are similar in all simulations (Figures 5 and 7), as the models are nested and the meteorological and surface conditions west of the Antarctic Peninsula are homogenous. This suggests that it is the representation of the detailed physics and model-resolved dynamics over the LCIS that are important to explain the sensitivity of the modelled foehn jets to different model resolutions.

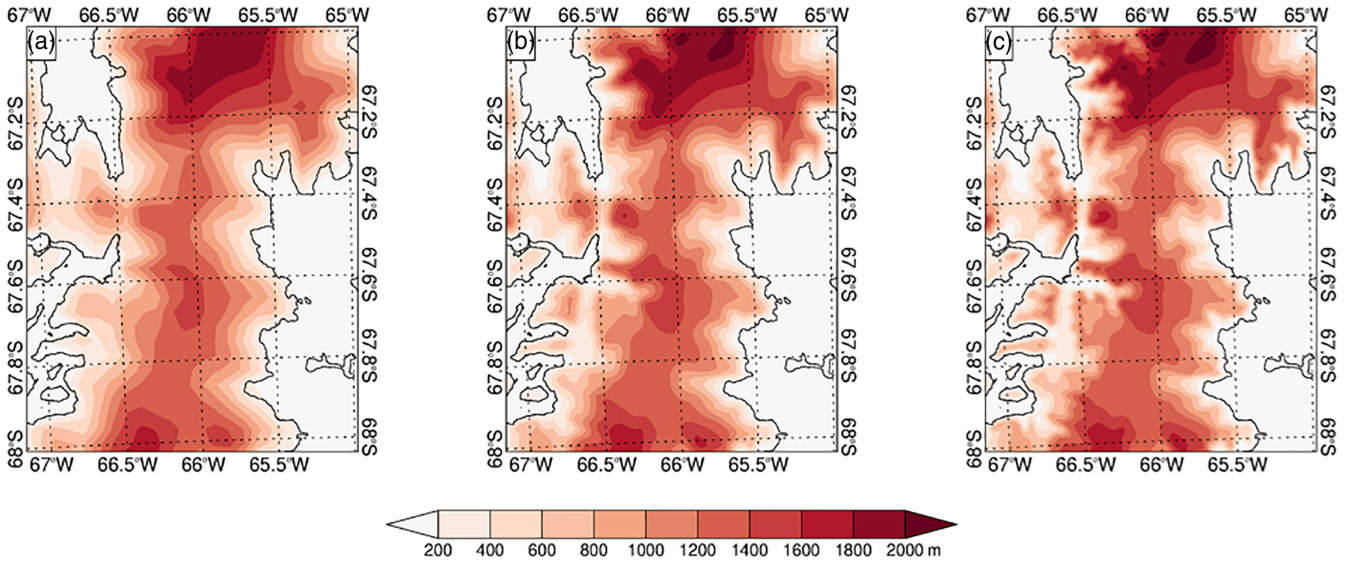

FIGURE 8 Comparison of the MetUM orography at (a) 4 km, (b) 1.5 km and (c) 0.5 km, for the Whirlwind Inlet region (labelled WI in Figure 1) [Colour figure can be viewed at wileyonlinelibrary.com]

To investigate this further, Figure 9 shows the simulated hourly accumulated temperature tendency profile at 1200 UTC on 27 January from both the dynamics and the total physics contribution at AWS1 (cf. Figure 4). The dominant contribution is from the dynamical temperature tendency, which shows mostly cooling throughout the atmosphere (Figure 9a). The 4 and 0.5 km models show a peak in cooling at around 80 m above the surface (although the values disagree markedly), while the 1.5 km model shows some warming between around 80 and 200 m, suggesting little evidence of resolution convergence. Additionally, between around 350 and 550 m the 4 km model shows warming, compared to the cooling shown by the 1.5 and 0.5 km models. The distinct peak in cooling at around 80 m broadly coincides with the region of highly stable air simulated by the models in Figure 4a, which capped the ground-based near-neutral layer. By contrast, the values for the total physics temperature tendency are largely insensitive to the range in horizontal resolution considered (Figure 9b). The total physics temperature tendency values show warming at the near-surface and some cooling above this, but a negligible contribution above around 200 m above the surface. The warming near the surface is perhaps responsible for the near-neutral well-mixed layer that is apparent in the simulations (Figure 4 and S1). Analogous results for 1800 UTC on 27 January show much smaller values of the dynamical temperature tendency in the lowest 150 m of the atmosphere, with relatively little model differences (Figure 9c). Above this region the differences in the dynamical temperature tendency between the different models are more considerable (cf. Figure 4b). By 1800 UTC the total physics temperature tendency shows warming in the lowest 200 m of the atmosphere (Figure 9d). Note that to investigate the representativeness of the hourly accumulated temperature tendency results (Figure 9), analogous results were produced but based on six-hourly accumulated temperature tendency values, that is, coinciding with more of the foehn wind event (not shown). Despite being smaller in size and characterised by less spread, the six- and one-hourly accumulated results are broadly similar.

At 1200 UTC the total physics temperature tendency is dominated by the contributions from boundary-layer subgrid-scale turbulent mixing and the diffusion scheme, with the boundary-layer scheme particularly responsible for the warming near the surface (Figure S3). Given that the simulated ground-based well-mixed layer is not apparent in the observations (Figure 4), this suggests that the sub-grid turbulent mixing is perhaps not accurate. Note that the positive contribution from the boundary-layer scheme is offset by negative values from the diffusion scheme, while the contributions from short-wave and long-wave radiation are much smaller than either of these (Figure S3). The warming at 1800 UTC due to the total physics temperature tendency in the lowest 200 m of the atmosphere is also mostly due to boundary-layer turbulent fluxes (Figure S3).

To further investigate the impact of the parameter choices for the stable boundary-layer scheme on the simulations, Figures 3, 4 and 9 contain results for the sensitivity experiment in which the "sharp" stability function was replaced with the "long-tail" stability function in the 4 km model. Despite the "long-tail" function giving significantly increased mixing under more stable

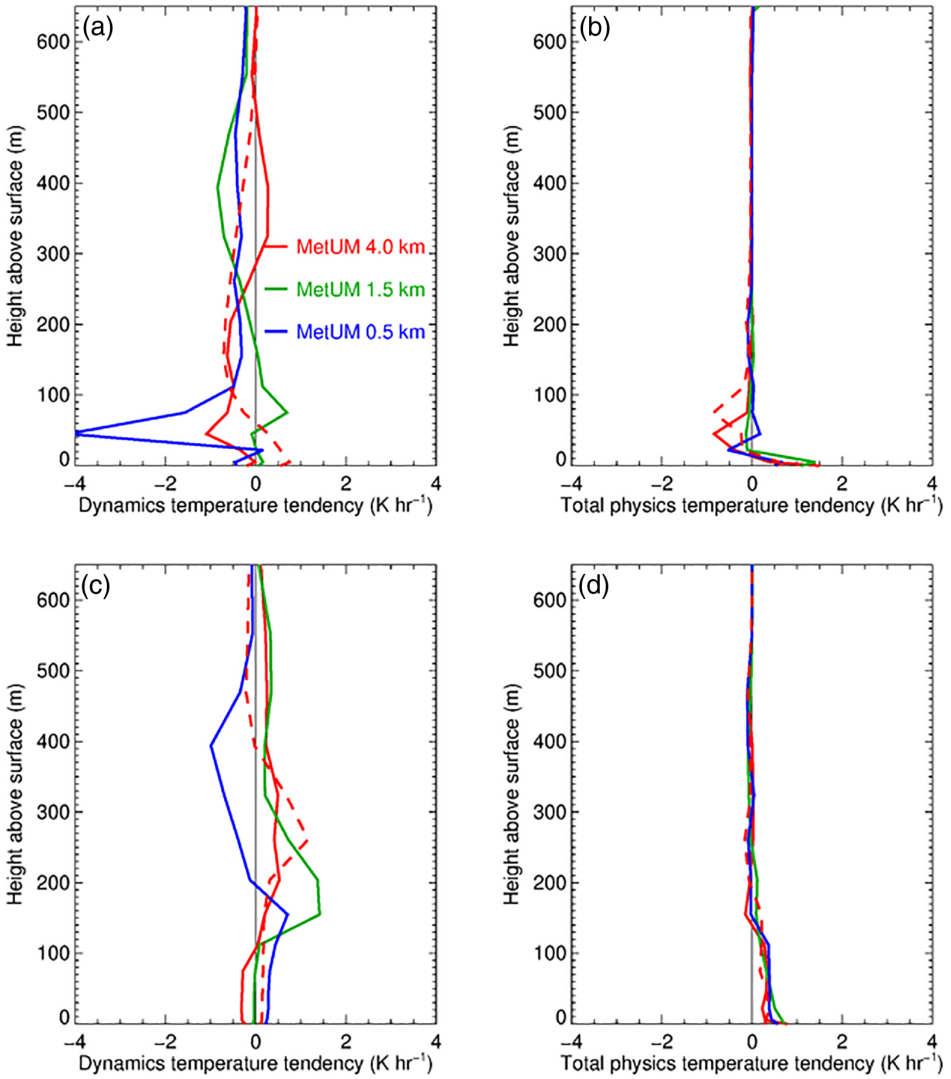

FIGURE 9 Comparison of the MetUM simulated vertical profile of the hourly accumulated (a,c) dynamical and (b,d) total physics temperature tendency (K·hr^{-1}), above AWS1 during the foehn wind case-study at (a,b) 1200 UTC (0900 LT) on 27 January 2011 and (c,d) 1800 UTC (1500 LT) on 27 January 2011 at horizontal resolutions of 4 km (red), 1.5 km (green) and 0.5 km (blue). These results are for the same time and location as the temperature profiles shown in Figure 4a. The dashed red line shows results for the MetUM 4 km simulation with the "long-tail" stability function for stable conditions. The MetUM results are based on hourly accumulated output saved at T + 12 hr and T + 18 hr from a run initialised at 0000 UTC on 27 January 2011 [Colour figure can be viewed at wileyonlinelibrary.com]

conditions (Brown *et al.*, 2008), which might therefore be expected to increase the mixing of warmer air at higher levels within the temperature inversion down to the near-surface (Orr *et al.*, 2014), the "long-tail" results broadly match the baseline 4 km results using the "sharp" function, that is, no appreciable near-surface warming. An exception is at the location of AWS3 (Figure 3c), which shows a nocturnal minimum temperature that is around 5 °C warmer for the "long-tail" run compared to the baseline 4 km run. Additionally, at the location of AWS1 the strength of the low-level wind jet at 1200 UTC on 27 January is up to 5 m·s^{-1} slower for the "long-tail" run compared to the baseline 4 km run (Figure 4c).

Although studies suggest that the representation of the boundary-layer processes that control the structure of the surface-based inversion/cold-air pool is comparatively insensitive to the vertical resolution (Billings *et al.*, 2006; Orr *et al.*, 2014), it is possible that the vertical resolution employed in these simulations (i.e. four vertical levels in the lowest 100 m of the atmosphere, arranged at 5, 22, 45 and 75 m) is insufficient to realistically capture the complex thermodynamic structure evident in the case-study. However, the sensitivity experiments described in Orr *et al.* (2014) showed that results from high-resolution MetUM simulations over the Antarctic were comparatively insensitive to a doubling of the number of vertical levels, suggesting that 16 vertical levels in the initial 1,000 m of the atmosphere is sufficient to resolve features of the stable boundary layer such as low-level inversions and wind jets (Orr *et al.*, 2005; 2014; Owinoh *et al.*, 2005).

Another likely contributor to the model error in near-surface temperature is the representation of cloud microphysics (King *et al.*, 2015; Gilbert *et al.*, 2020; 2021). Figure 10 compares the simulated low-level cloud fraction at 1200 UTC on 27 January with cloud data from MODIS at 1309 UTC. The MODIS data show extensive cloud over the eastern regions of the LCIS, and cloud-free conditions over the western and central regions. By contrast, the MetUM

simulations at all resolutions show cloud-free conditions extending completely across the LCIS between 67° and 68°S (and areas of cloud to the north and south of this over the eastern regions of the LCIS), that is, there is less cloud across the eastern section of the LCIS in the MetUM simulation than in the observations. Note that the MetUM simulated medium- and upper-level cloud fraction showed cloud-free conditions over the LCIS at 1200 UTC on 27 January (not shown).

Figure 11 suggests that this may have some impact on the simulation of the surface radiation components compared to the measured values from AWS1, which is situated in the eastern section of the LCIS (Figure 1). For example, up to 1500 UTC on 27 January the results indicate that the model overestimates (underestimates) the amount of incoming short-wave (long-wave) radiation, which is consistent with the simulations underestimating the cloud cover (Figure 10), as well as the simulation of excessively low temperatures. After 1800 UTC the model values are in much better agreement with the observations. Despite this, the total physics temperature tendency was dominated by the contribution from the boundary-layer scheme and diffusion, with the contribution from short-wave and long-wave radiation much smaller than either of these (Figure S3). The radiative temperature tendencies are due to the divergence of the radiative fluxes at an atmospheric level, which will generally be much smaller than the turbulent flux divergence within the boundary layer. However, errors in the surface values of the radiative fluxes will cause errors in the surface energy balance, hence in surface temperature, hence in turbulent heat fluxes and atmospheric temperature. Additionally, the values of radiation at the surface for the 4, 1.5 and 0.5 km models are all largely similar (Figure 11).

Finally, deficiencies in the representation of the snow/ice surface using the "zero-layer" scheme would also impact the near-surface air temperature. For example, Walters *et al.* (2019) showed that the near-surface air over the Greenland ice sheet was warmer using the multi-layer snow scheme compared to the "zero-layer" scheme. This finding perhaps suggests that use of the "zero-layer" scheme could be at least partially responsible for the 4 km model struggling to simulate daytime temperatures above freezing (Figure 2).

5 | CONCLUSIONS

This study evaluates the ability of high-resolution atmospheric models to represent the interaction of foehn with a cold-air pool over the LCIS by examining MetUM simulations of a case-study event at grid spacings of 4, 1.5 and 0.5 km. During the event, the simulated nocturnal minimum temperature was around 8 °C too low over the LCIS (Figures 2 and 3), with no reduction in the size of the cold bias with increasing resolution. It was found that the representation of the key features associated with foehn (such as low-level upstream blocking, leeside hydraulic jump, upper-level wave breaking, downslope winds) were comparatively insensitive to resolution in the 4 to 0.5 km range, although the 0.5 km simulation shows a slightly sharper and larger hydraulic jump (Figure 7). In particular, the foehn winds at the base of the Antarctic Peninsula only appear to influence the local/western parts of the LCIS, suggesting that they are not directly responsible for the contemporaneous large errors in near-surface temperature over the LCIS (Figure 3) and difficulties in realistically representing the structure of the cold-air pool (Figure 4), which did not improve with increased resolution.

By contrast, the simulation of the pattern and strength of the low-level foehn jets over the LCIS showed considerable dependence on grid spacing, although no evidence of convergence (Figures 5 and 6). The foehn jets are important as they can influence the erosion of cold-air pools/ground-based temperature inversions by wind-induced turbulent mixing (Figures 4 and 9), and therefore require to be considered alongside sub-grid turbulent mixing (Zhong and Chow, 2013; Elvidge *et al.*, 2015; Vosper *et al.*, 2018). We stress that this work suggests that the models struggle to capture both of these aspects (Mahrt, 1998; Tastula and Vihma, 2011; Holtslag *et al.*, 2013; Zardi and Whiteman, 2013; Steeneveld, 2014) and both are thus likely candidates for causing/influencing the errors in near-surface temperature.

Future work could continue to focus on the interaction of foehn and cold-air pools over the LCIS. One aspect of this could be to investigate whether the resolution-dependent sensitivities revealed in this study for the MetUM are apparent in other non-hydrostatic regional atmospheric models, such as the polar-optimised WRF or CCLM models. The behaviour of the boundary-layer schemes in other atmospheric models under such extreme and testing conditions could also be investigated (Teixeira *et al.*, 2008; Holtslag *et al.*, 2013; Zhong and Chow, 2013). Another aspect to look at further is the treatment of horizontal diffusion (Billings *et al.*, 2006), as this was shown to offset the temperature tendency from the boundary-layer scheme (Figure S3). For the MetUM, the possible role of its sub-grid drainage scheme could be investigated, which is dependent on the subgrid-scale orography fields (Bush *et al.*, 2020). The limitations of the representation of the snow/ice surface using the "zero-layer" scheme in the MetUM simulations is another area of possible investigation, as the treatment of surface and subsurface processes are important for the atmospheric boundary layer and cold-pool

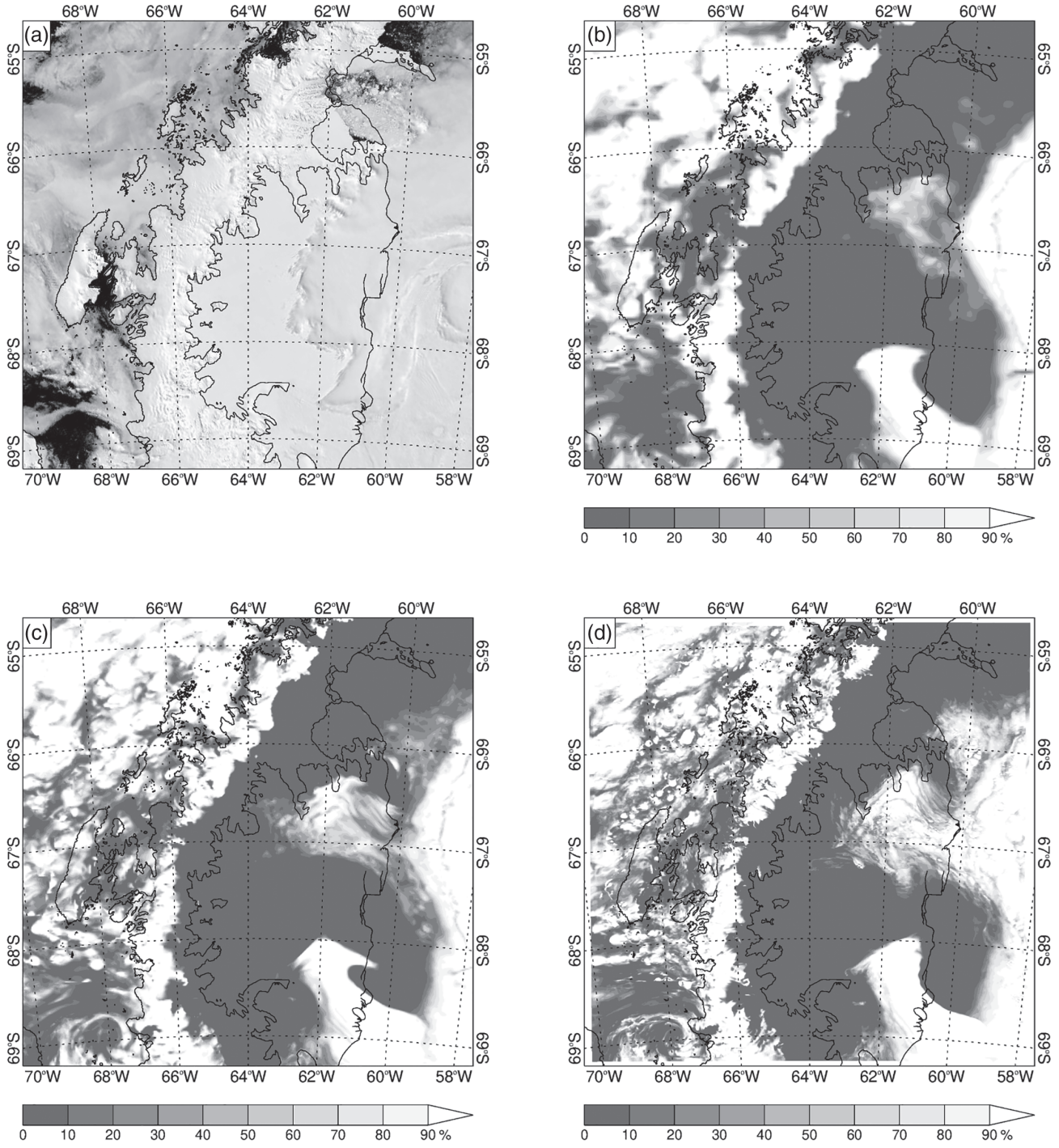

FIGURE 10 Comparison of the (a) MODIS observed cloud cover at 1309 UTC on 27 January 2011 with the MetUM simulated low-level cloud fraction (%) at a horizonal resolution of (b) 4 km, (c) 1.5 km and (d) 0.5 km, at 1200 UTC (0900 LT) on 27 January 2011. The MODIS image shows extensive cloud over the eastern regions of the LCIS, and cloud-free conditions over the western and central regions. By contrast, the MetUM simulations show cloud-free conditions extending completely across the LCIS between 67° and 68°S, as well as over the western regions of the LCIS. The MetUM results are based on instantaneous output saved at T + 12 hr from a run initialised at 0000 UTC on 27 January 2011

development (Ettema *et al.*, 2010; Walters *et al.*, 2019). For example, the polar-optimised models RACMO2 and MAR both use a physically realistic multi-layer snow model and snow albedo scheme (Ettema *et al.*, 2010; Datta *et al.*, 2019). For the MetUM, the impact of this could be investigated by replacing the "zero-layer" model with a multi-layer snow model, which is another option in the JULES land-surface scheme (Walters *et al.*, 2019).

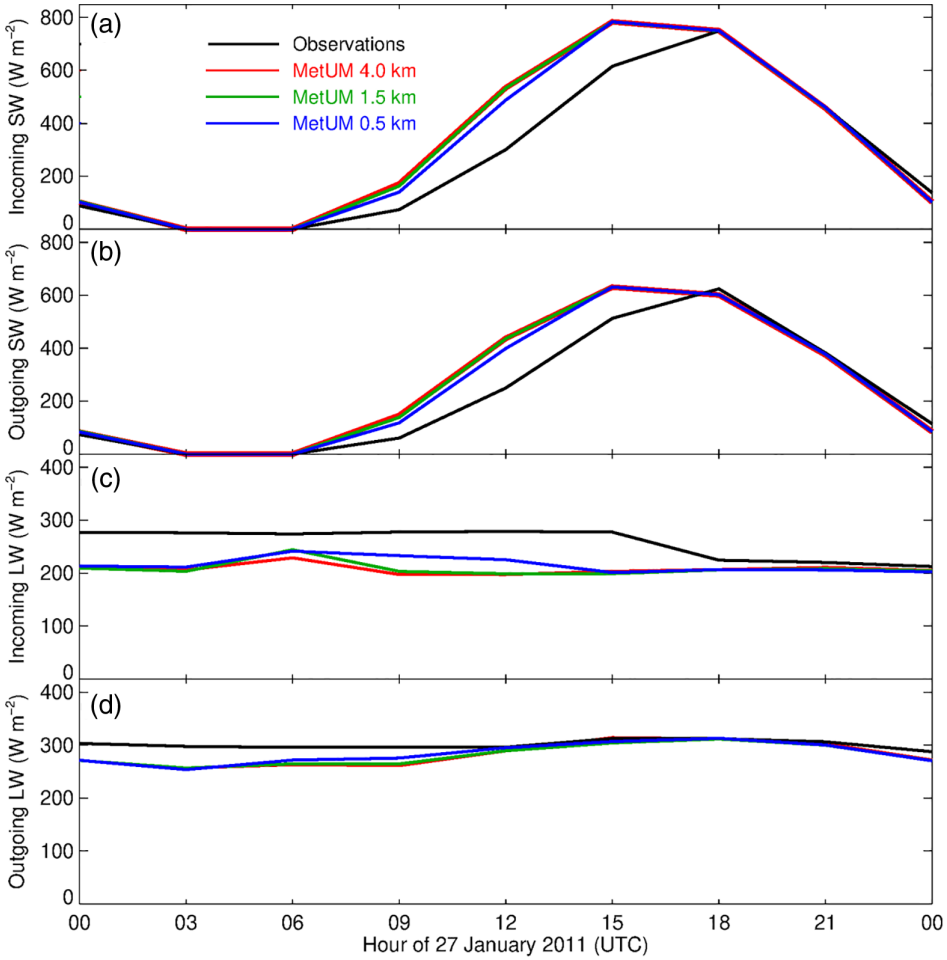

FIGURE 11 Comparison of measured (black) and MetUM simulated (a) incoming short-wave, (b) outgoing short-wave, (c) incoming long-wave and (d) outgoing long-wave radiation ($W \cdot m^{-2}$), at horizontal resolutions of 4 km (red), 1.5 km (green) and 0.5 km (blue), during the foehn wind case-study from 0000 to 2400 UTC on 27 January 2011. The MetUM results are based on the combination of instantaneous output from runs initialised at 1200 UTC on 26 January 2011 (contributing fields at T + 12, T + 15, T + 18, T + 21 and T + 24 hr) and 0000 UTC on 27 January 2011 (contributing fields at T + 15, T + 18, T + 21 and T + 24 hr) [Colour figure can be viewed at wileyonlinelibrary.com]

Finally, the use of large-eddy simulations at resolutions of the order of 100 m or finer that can better resolve both the horizontal and vertical transport processes could be used to clarify their relative importance (e.g. Zhong and Chow, 2013; Wagner *et al.*, 2014; Vosper *et al.*, 2018; Xue *et al.*, 2020).

ACKNOWLEDGEMENTS

This study is dedicated to Konrad Steffen, who was a co-author on an earlier draft of this manuscript, but very sadly died in 2020. Konrad was the Director of the Swiss Federal Institute for Forest, Snow and Landscape Research (WSL), and former Director of the Cooperative Institute for Research in Environmental Sciences (CIRES), University of Colorado, who operated AWS 3, 4 and 5. We are grateful for the advice given by Adrian Lock on the model boundary-layer scheme and by Richard Essery on the surface scheme. This study was supported by the UK Natural Environment Research Council (NERC) under grant NE/G014124/1 "Orographic Flows and the Climate of the Antarctic Peninsula (OFCAP)". We are grateful for the expert comments by two anonymous referees on an earlier version of this article which significantly expanded its scope, in particular by suggesting that the interaction between the foehn event and the cold-air pool be examined in much more detail.

AUTHOR CONTRIBUTIONS

Andrew Orr: Conceptualization; formal analysis; investigation; methodology; validation; visualization; writing - original draft; writing-review & editing. **Amelie Kirchgaessner:** Data curation; resources; writing-review & editing. **John King:** Funding acquisition; project administration; writing-review & editing. **Tony Phillips:** Data curation; resources; visualization; writing-review & editing. **Ella Gilbert:** Methodology; writing-review & editing. **Andrew Elvidge:** Conceptualization; methodology; writing-review & editing. **Mark Weeks:** Conceptualization; methodology; resources; writing-review & editing. **Alan Gadian:** Conceptualization; writing-review & editing. **Peter Kuipers Munneke:** Data curation; methodology; writing-review & editing. **Michiel Van den Broeke:** Methodology; writing-review & editing. **Stuart Webster:** Methodology; resources; writing-review & editing. **Daniel McGrath:** Data curation; writing-review & editing.

DATA AVAILABILITY STATEMENT

The AWS1 and 2 data used in this study are available for download from the PANGAEA data repository: doi: 10.1594/PANGAEA.910484. The AWS3, 4 and 5 data are available for download from the USAP-DC (U.S. Antarctic Program Data Center) website: https://10.15784/601445 (McGrath *et al.*, 2021). The MODIS cloud data are available from the NASA (National Aeronautics and Space Administration) website: https://modis.gsfc.nasa.gov/data/dataprod/mod06.php. The radiosonde observations from the AWS1 site are available from the CEDA (Centre for Environmental Data Analysis) website: http://10.5285/5c8bc811-edab-4e1d-bceb-afb9623b9afa (Kirchgaessner *et al.*, 2014). The MetUM model output is available from the UK PDC (UK Polar Data Centre) website: https://10.5285/c5cc491e-7119-4500-b05a-e5e34274438f (Orr and Phillips, 2021). We acknowledge use of the SCAR (Scientific Committee on Antarctic Research) Antarctic Digital Database, which is accessed here: https://www.add.scar.org/.

ORCID

Andrew Orr https://orcid.org/0000-0001-5111-8402

REFERENCES

Anderson, P.S. (1994) A method for rescaling humidity sensors at temperatures well below freezing. *Journal of Atmospheric and Oceanic Technology*, 11, 1388–1391. https://doi.org/10.1175/1520-0426(1994)011<1388:AMFRHS>2.0.CO;2.

Alexander, S.P., Orr, A., Webster, S. and Murphy, D.J. (2017) Observations and fine-scale model simulations of gravity waves over Davis, East Antarctica (69°S, 78°E). *Journal of Geophysical Research: Atmospheres*, 122, 7355–7370. https://doi.org/10.1002/2017JD026615.

Bacmeister, J.T., Schoeberl, M.R., Lait, L.R., Newman, P.A. and Bruce, G. (1990) ER-2 mountain wave encounter over Antarctica: evidence for blocking. *Geophysical Research Letters*, 17, 81–84. https://doi.org/10.1029/GL017i001p00081.

Baines, P.G. and Smith, R.B. (1993) Upstream stagnation points in stratified flow past obstacles. *Dynamics of Atmospheres and Oceans*, 18, 105–113. https://doi.org/10.1016/0377-0265(93)90005-R.

Banwell, A.F., MacAyeal, D.R. and Sergienko, O.V. (2013) Breakup of the Larsen B ice shelf triggered by chain reaction drainage of supraglacial lakes. *Geophysics Research Letters*, 40, 5872–5876. https://doi.org/10.1002/2013GL057694.

Best, M.J., Pryor, M., Clark, D.B., Rooney, G.G., Essery, R.L.H., Menard, C.B., Edwards, J.M., Hendry, M.A., Porson, A., Gedney, N., Mercado, L.M., Sitch, S., Blyth, E., Boucher, O., Cox, P.M., Grimmond, C.S.B. and Harding, R.J. (2011) The joint UK Land Environment Simulator (JULES), model description – Part 1: Energy and water fluxes. *Geoscientific Model Development*, 4, 677–699. https://doi.org/10.5194/gmd-4-677-2011.

Bevan, S.L., Luckman, A., Hubbard, B., Kulessa, B., Ashmore, D., Kuipers Munneke, P., O'Leary, M., Booth, A., Sevestre, H. and McGrath, D. (2017) Centuries of intense surface melt on Larsen C ice shelf. *The Cryosphere*, 11, 2743–2753. https://doi.org/10.5194/tc-11-2743-2017.

Beljaars, A.C.M. and Holtslag, A.A.M. (1991) Flux parameterization over land surfaces for atmospheric models. *Journal of Applied Meteorology*, 30, 327–341. https://doi.org/10.1175/1520-0450(1991)030<0327:FPOLSF>2.0.CO;2.

Bevan, S.L., Luckman, A.J., Kuipers Munneke, P., Hubbard, B., Kulessa, B. and Ashmore, D.W. (2018) Decline in surface melt duration on Larsen C ice shelf revealed by the advanced scatterometer (ASCAT). *Earth and Space Science*, 5, 578–591. https://doi.org/10.1029/2018EA000421.

Billings, B.J., Grubišić, V. and Borys, R.D. (2006) Maintenance of a valley cold pool: a numerical study. *Monthly Weather Review*, 134, 2266–2278. https://doi.org/10.1175/MWR3180.1.

Blackadar, A.K. (1957) Boundary layer wind maxima and their significance for the growth of nocturnal inversions. *Bulletin of the American Meteorological Society*, 38, 283–290. https://doi.org/10.1175/1520-0477-38.5.283.

Brown, A.R., Beare, R.J., Edwards, J.M., Lock, A.P., Keogh, S.J., Milton, S.F. and Walters, D.N. (2008) Upgrades to the boundary-layer scheme in the Met Office numerical weather prediction model. *Boundary-Layer Meteorology*, 128, 117–132. https://doi.org/10.1007/s10546-008-9275-0.

Bush, M., Allen, T., Bain, C., Boutle, I., Edwards, J., Finnenkoetter, A., Franklin, C., Hanley, K., Lean, H., Lock, A., Manners, J., Mittermaier, M., Morcrette, C., North, R., Petch, J., Short, C., Vosper, S., Walters, D., Webster, S., Weeks, M., Wilkinson, J., Wood, N. and Zerroukat, M. (2020) The first Met Office unified model–JULES regional atmosphere and land configuration, RAL1. *Geoscientific Model Development*, 13, 1999–2029. https://doi.org/10.5194/gmd-13-1999-2020.

Cape, M.R., Vernet, M., Skvarca, P., Marinsek, S., Scambos, T. and Domack, E. (2015) Foehn winds link climate-driven warming to ice shelf evolution in Antarctica. *Journal of Geophysical Research: Atmospheres*, 120, 11037–11057. https://doi.org/10.1002/2015JD023465.

Datta, R.T., Tedesco, M., Fettweis, X., Agosta, C., Lhermitte, S., Lenaerts, J. and Wever, N. (2019) The effect of foehn-induced surface melt on firn evolution over the northeast Antarctic Peninsula. *Geophysical Research Letters*, 46, 3822–3831. https://doi.org/10.1029/2018GL080845.

Dee, D.P., Uppala, S.M., Simmons, A.J., Berrisford, P., Poli, P., Kobayashi, S., Andrae, U., Balmaseda, M.A., Balsamo, G., Bauer, P., Bechtold, P., Beljaars, A.C.M., van de Berg, L., Bidlot, J., Bormann, N., Delsol, C., Dragani, R., Fuentes, M., Geer, A.J., Haimberger, L., Healy, S.B., Hersbach, H., Hólm, E.V., Isaksen, L., Kållberg, P., Köhler, M., Matricardi, M., McNally, A.P., Monge-Sanz, B.M., Morcrette, J.J., Park, B.K., Peubey, C., de Rosnay, P., Tavolato, C., Thépaut, J.-N. and Vitart, F. (2011) The ERA-Interim reanalysis: configuration and performance of the data assimilation system. *Quarterly Journal of the Royal Meteorological Society*, 137(656), 553–597. https://doi.org/10.1002/qj.828.

Dell, R., Arnold, N., Willis, I., Banwell, A., Williamson, A., Pritchard, H. and Orr, A. (2020) Lateral meltwater transfer across an Antarctic ice shelf. *The Cryosphere*, 14, 2313–2330. https://doi.org/10.5194/tc-14-2313-2020.

Elvidge, A.D., Renfrew, I.A., King, J.C., Orr, A., Lachlan-Cope, T.A., Weeks, M. and Gray, S.L. (2015) Foehn jets over the Larsen C

ice shelf, Antarctica. *Quarterly Journal of the Royal Meteorological Society*, 141(688), 698–713. https://doi.org/10.1002/qj.2382.

Elvidge, A.D., Renfrew, I.A., King, J.C., Orr, A. and Lachlan-Cope, T.A. (2016) Foehn warming distributions in nonlinear and linear flow regimes: a focus on the Antarctic Peninsula. *Quarterly Journal of the Royal Meteorological Society*, 142(695), 618–631. https://doi.org/10.1002/qj.2489.

Elvidge, A.D., Kuipers Munneke, P., King, J.C., Renfrew, I.A. and Gilbert, E. (2020) Atmospheric drivers of melt on Larsen C ice shelf: surface energy budget regimes and the impact of foehn. *Journal of Geophysical Research: Atmospheres*, 125(17), e2020JD032463. https://doi.org/10.1029/2020JD032463.

Ettema, J., van den Broeke, M.R., van Meijgaard, E., van de Berg, W.J., Box, J.E. and Steffen, K. (2010) Climate of the Greenland ice sheet using a high-resolution climate model – Part 1: Evaluation. *The Cryosphere*, 4, 511–527. https://doi.org/10.5194/tc-4-511-2010.

Flamant, C., Drobinski, P., Furger, M., Chimani, B., Tschannett, S., Steinacker, R., Protat, A., Richner, H., Gubser, S. and Häberli, C. (2006) Föhn/cold-pool interactions in the Rhine valley during MAP IOP 15. *Quarterly Journal of the Royal Meteorological Society*, 132(621), 3035–3058. https://doi.org/10.1256/qj.06.36.

Gilbert, E.M., Orr, A., King, J.C., Renfrew, I.A., Lachlan-Cope, T.A., Field, P.F. and Boutle, I.A. (2020) Summertime cloud phase strongly influences surface melting on the Larsen C ice shelf, Antarctica. *Quarterly Journal of the Royal Meteorological Society*, 146(729), 1575–1589. https://doi.org/10.1002/qj.3753.

Grosvenor, D.P., King, J.C., Choularton, T.W. and Lachlan-Cope, T. (2014) Downslope föhn winds over the Antarctic Peninsula and their effect on the Larsen ice shelves. *Atmospheric Chemistry and Physics*, 14, 9481–9509. https://doi.org/10.5194/acp-14-9481-2014.

Haid, M., Gohm, A., Umek, L., Ward, H.C., Muschinski, T., Lehner, L. and Rotach, M.W. (2020) Foehn–cold pool interactions in the Inn Valley during PIANO IOP2. *Quarterly Journal of the Royal Meteorological Society*, 146(728), 1232–1263. https://doi.org/10.1002/qj.3735.

Holtslag, A.A.M., Svensson, G., Baas, P., Basu, S., Beare, B., Beljaars, A.C.M., Bosveld, F.C., Cuxart, J., Lindvall, J., Steeneveld, G.J., Tjernström, M. and Van De Wiel, B.J.H. (2013) Stable atmospheric boundary layers and diurnal cycles: challenges for weather and climate models. *Bulletin of the American Meteorological Society*, 94, 1691–1706. https://doi.org/10.1175/BAMS-D-11-00187.1.

Hunt, J.C.R. and Snyder, W.H. (1980) Experiments on stably and neutrally stratified flow over a model three dimensional hill. *Journal of Fluid Mechanics*, 96, 671–704. https://doi.org/10.1017/S0022112080002303.

Kalnay, E. (2002) *Atmospheric Modeling, Data Assimilation and Predictability*. Cambridge, UK: Cambridge University Press.

King, J.C., Lachlan-Cope, T.A., Ladkin, R.S. and Weiss, A. (2008) Airborne measurements in the stable boundary layer over the Larsen ice shelf. Antarctica. *Boundary-Layer Meteorology*, 127, 413–428. https://doi.org/10.1007/s10546-008-9271-4.

King, J.C., Gadian, A., Kirchgaessner, A., Kuipers Munneke, P., Lachlan-Cope, T.A., Orr, A., Reijmer, C., van den Broeke, M.R., van Wessem, J.M. and Weeks, M. (2015) Validation of the summertime surface energy budget of Larsen C ice shelf (Antarctica) as represented in three high-resolution atmospheric models. *Journal of Geophysical Research: Atmospheres*, 120, 1335–1347. https://doi.org/10.1002/2014JD022604.

Kirchgaessner, A., Kuipers Munneke, P. and King, J. C. (2014) *Radiosonde data from the orographic flows and the climate of the Antarctic peninsula (OFCAP) project (January 2011)*. NCAS British Atmospheric Data Centre, 23 September 2014. doi:https://doi.org/10.5285/5c8bc811-edab-4e1d-bceb-afb9623b9afa.

Kirchgaessner, A., King, J. and Gadian, A. (2019) The representation of föhn events to the east of the Antarctic Peninsula in simulations by the Antarctic mesoscale prediction system. *Journal of Geophysical Research: Atmospheres*, 124, 13663–13679. https://doi.org/10.1029/2019JD030637.

Knist, S., Goergen, K. and Simmer, C. (2020) Effects of land surface inhomogeneity on convection-permitting WRF simulations over Central Europe. *Meteorology and Atmospheric Physics*, 132, 53–69. https://doi.org/10.1007/s00703-019-00671-y.

Kuipers Munneke, P., van den Broeke, M., King, J.C., Gray, T. and Reijmer, C. (2012) Near-surface climate and surface energy budget of Larsen C Ice Shelf, Antarctic Peninsula. *The Cryosphere*, 6, 353–363. https://doi.org/10.5194/tc-6-353-2012.

Kuipers Munneke, P., Ligtenberg, S.R.M., van den Broeke, M.R. and Vaughan, D.G. (2014) Firn air depletion as a precursor of Antarctic ice-shelf collapse. *Journal of Glaciology*, 60, 205–214. https://doi.org/10.3189/2014JoG13J183.

Kuipers Munneke, P., Luckman, A.J., Bevan, S.L., Smeets, C.J.P.P., Gilbert, E., van den Broeke, M.R., Wang, W., Zender, C., Hubbard, B., Ashmore, D., Orr, A., King, J.C. and Kulessa, B. (2018) Intense winter surface melt on an Antarctic ice shelf. *Geophysical Research Letters*, 45, 7615–7623. https://doi.org/10.1029/2018GL077899.

Liu, H., Jezek, K., Li, B. and Zhao, Z. (2015) *Radarsat Antarctic Mapping Project Digital Elevation Model Version 9*. Boulder, CO: NASA National Snow and Ice Data Center Distributed Active Archive Center. https://doi.org/10.5067/8JKNEW6BFRVD.

Luckman, A., Elvidge, A., Jansen, D., Kulessa, B., Kuipers Munneke, P., King, J.C. and Barrand, N.E. (2014) Surface melt and ponding on the Larsen C ice shelf and the impact of föhn winds. *Antarctic Science*, 25, 625–635. https://doi.org/10.1017/S0954102014000339.

Mahrt, L. (1998) Stratified atmospheric boundary layers and breakdown of models. *Theoretical and Computational Fluid Dynamics*, 11, 263–279. https://doi.org/10.1007/s001620050093.

Marshall, G.J., Orr, A., van Lipzig, N.P.M. and King, J.C. (2006) The impact of a changing Southern Hemisphere annular mode on Antarctic Peninsula summer temperatures. *Journal of Climate*, 19, 5388–5404. https://doi.org/10.1175/JCLI3844.1.

McGrath, D., Nicolas, B. and Konrad, S. (2021) *Larsen C automatic weather station data 2008–2011*. U.S. Antarctic Program (USAP) Data Center. https://doi.org/10.15784/601445.

Mottram, R., Hansen, N., Kittel, C., van Wessem, J. M., Agosta, C., Amory, C., Boberg, F., van de Berg, W.J., Fettweis, X., Gossart, A., van Lipzig, N.P.M., van Meijgaard, E., Orr, A., Phillips, T., Webster, S., Simonsen, S.B. and Souverijns, N. (2021) What is the surface mass balance of Antarctica? An intercomparison of regional climate model estimates. *The Cryosphere*, 15, 3751–3784 https://doi.org/10.5194/tc-15-3751-2021.

Orr, A., Cresswell, D., Marshall, G.J., Hunt, J.C.R., Sommeria, J., Wang, C.G. and Light, M. (2004) A "low-level" explanation for the recent large warming trend over the western Antarctic Peninsula involving blocked winds and changes in zonal circulation.

Geophysical Research Letters, 31, L06204. https://doi.org/10.1029/2003GL019160.

Orr, A., Hunt, J.C.R., Capon, R., Sommeria, J., Cresswell, D. and Owinoh, A. (2005) Coriolis effects on wind jets and cloudiness along coasts. *Weather*, 60(10), 291–299. https://doi.org/10.1256/wea.219.04.

Orr, A., Marshall, G.J., Hunt, J.C.R., Sommeria, J., Wang, C., van Lipzig, N., Cresswell, D. and King, J.C. (2008) Characteristics of airflow over the Antarctic peninsula and its response to recent strengthening of westerly circumpolar winds. *Journal of the Atmospheric Sciences*, 65, 1396–1413. https://doi.org/10.1175/2007JAS2498.1.

Orr, A., Phillips, T., Webster, S., Elvidge, A., Weeks, M., Hosking, S. and Turner, J. (2014) Met Office Unified Model high-resolution simulations of a strong wind event in Antarctica. *Quarterly Journal of the Royal Meteorological Society*, 140(684), 2287–2297. https://doi.org/10.1002/qj.2296.

Orr, A., Hosking, J.S., Hoffmann, L., Keeble, J., Dean, S.M., Roscoe, H.K., Abraham, L., Vosper, S. and Phillips, T. (2015) Inclusion of mountain wave-induced cooling for the formation of PSCs over the Antarctic Peninsula in a chemistry-climate model. *Atmospheric Chemistry and Physics*, 15, 1071–1086. https://doi.org/10.5194/acp-15-1071-2015.

Orr, A. and Phillips, T. (2021) *Kilometre and sub-kilometre scale atmosphere-only model simulations using the Met Office Unified Model of a foehn wind event over the Larsen C Ice Shelf, Antarctic Peninsula on 27 January 2011 (Version 1.0) [Data set]*. NERC EDS UK Polar Data Centre. https://doi.org/10.5285/c5cc491e-7119-4500-b05a-e5e34274438f.

Owinoh, A.Z., Hunt, J.C.R., Orr, A., Clark, P., Klein, R., Fernando, H.J.S. and Nieuwstadt, F.T.M. (2005) Effects of changing surface heat flux on the atmospheric boundary-layer flow over flat terrain. *Boundary-Layer Meteorology*, 116, 331–361. https://doi.org/10.1007/s10546-004-2819-z.

Platnick, S., Ackerman, S., King, M., Wind, G., Meyer, K., Menzel, P., Frey, R., Holz, R., Baum, B. and Yang, P. (2015) *MODIS atmosphere L2 cloud product (06_L2)*. NASA MODIS Adaptive Processing System, Goddard Space Flight Center. doi:https://doi.org/10.5067/MODIS/MOD06_L2.006.

Jakobs, C., Reijmer, C., Smeets, C., Trusel, L., van de Berg, W., van den Broeke, M. and van Wessem, J. (2020) A benchmark dataset of *in situ* Antarctic surface melt rates and energy balance. *Journal of Glaciology*, 66, 291–302. https://doi.org/10.1017/jog.2020.6.

Rott, H., Skvarça, P. and Nagler, T. (1996) Rapid collapse of northern Larsen ice shelf, Antarctica. *Science*, 271, 788–792. https://doi.org/10.1126/science.271.5250.788.

Scambos, T.A., Hulbe, C., Fahnestock, M. and Bohlander, J. (2000) The link between climate warming and break-up of ice shelves in the Antarctic Peninsula. *Journal of Glaciology*, 46, 516–530. https://doi.org/10.3189/172756500781833043.

Shutts, G.J. and Vosper, S.B. (2011) Stratospheric gravity waves revealed in NWP model forecasts. *Quarterly Journal of the Royal Meteorological Society*, 137(655), 303–317. https://doi.org/10.1002/qj.763.

Smeets, P.C.J.P., Kuipers Munneke, P., van As, D., van den Broeke, M.R., Boot, W., Oerlemans, H., Snellen, H., Reijmer, C.H. and van de Wal, R.S.W. (2018) The K-transect in west Greenland: automatic weather station data (1993–2016). *Arctic, Antarctic, and Alpine Research*, 50(1), S100002. https://doi.org/10.1080/15230430.2017.1420954.

Smith, R.B. (1989) Hydrostatic airflow over mountains. *Advances in Geophysics*, 31, 1–41. https://doi.org/10.1016/S0065-2687(08)60052-7.

Steeneveld, G.-J. (2014) Current challenges in understanding and forecasting stable boundary layers over land and ice. *Frontiers in Environmental Science*, 2, 1–6. https://doi.org/10.3389/fenvs.2014.00041.

Tang, Y., Lean, H.W. and Bornemann, J. (2013) The benefits of the Met Office variable resolution NWP model for forecasting convection. *Meteorological Applications*, 20, 417–426. https://doi.org/10.1002/met.1300.

Tastula, E.-M. and Vihma, T. (2011) WRF model experiments on the Antarctic atmosphere in winter. *Monthly Weather Review*, 139, 1279–1291. https://doi.org/10.1175/2010MWR3478.1.

Teixeira, J., Stevens, B., Bretherton, C.S., Cederwall, R., Doyle, J.D., Golaz, J.C., Holtslag, A.A.M., Klein, S.A., Lundquist, J.K., Randall, D.A., Siebesma, A.P. and Soares, P.M.M. (2008) Parameterization of the atmospheric boundary layer: a view from just above the inversion. *Bulletin of the American Meteorological Society*, 89, 453–458. https://doi.org/10.1175/BAMS-89-4-453.

Thorpe, A.J. and Guymer, T.H. (1977) The nocturnal jet. *Quarterly Journal of the Royal Meteorological Society*, 103(438), 633–653. https://doi.org/10.1002/qj.49710343809.

Trusel, L.D., Frey, K.E., Das, S.B., Karnauskas, K.B., Kuipers Munneke, P., van Meijgaard, E. and van den Broeke, M.R. (2015) Divergent trajectories of Antarctic surface melt under two twenty-first century climate scenarios. *Nature Geoscience*, 8, 927–932. https://doi.org/10.1038/ngeo2563.

Turton, J.V., Kirchgaessner, A., Ross, A.N. and King, J.C. (2017) Does high-resolution modelling improve the spatial analysis of föhn flow over the Larsen C ice shelf? *Weather*, 72(7), 192–196. https://doi.org/10.1002/wea.3028.

Turton, J.V., Kirchgaessner, A., Ross, A.N. and King, J.C. (2018) The spatial distribution and temporal variability of föhn winds over the Larsen C ice shelf, Antarctica. *Quarterly Journal of the Royal Meteorological Society*, 144(713), 1169–1178. https://doi.org/10.1002/qj.3284.

Turton, J.V., Kirchgaessner, A., Ross, A.N., King, J.C. and Kuipers Munneke, P. (2020) The influence of föhn winds on annual and seasonal surface melt on the Larsen C ice shelf, Antarctica. *The Cryosphere*, 14, 4165–4180. https://doi.org/10.5194/tc-14-4165-2020.

van Lipzig, N.P.M., Marshall, G.J., Orr, A. and King, J.C. (2008) The relationship between the Southern Hemisphere annular mode and Antarctic Peninsula summer temperatures: analysis of a high-resolution model climatology. *Journal of Climate*, 21, 1649–1668. https://doi.org/10.1175/2007JCLI1695.1.

van den Broeke, M.R., van Lipzig, N.P.M. and van Meijgaard, E. (2002) Momentum budget of the East Antarctic atmospheric boundary layer: results of a regional climate model. *Journal of the Atmospheric Sciences*, 59, 3117–3129. https://doi.org/10.1175/1520-0469(2002)059<3117:MBOTEA>2.0.CO;2.

van Wessem, J.M., Ligtenberg, S.R.M., Reijmer, C.H., van de Berg, W.J., van den Broeke, M.R., Barrand, N.E., Thomas, E.R., Turner, J., Wuite, J., Scambos, T.A. and van Meijgaard, E. (2016) The modelled surface mass balance of the Antarctic peninsula at 5.5 km

horizontal resolution. *The Cryosphere*, 10, 271–285. https://doi.org/10.5194/tc-10-271-2016.

Vosper, S.B., Ross, A.N., Renfrew, I.A., Sheridan, P., Elvidge, A.D. and Grubišić, V. (2018) Current challenges in orographic flow dynamics: turbulent exchange due to low-level gravity-wave processes. *Atmosphere*, 9(9), 361. https://doi.org/10.3390/atmos9090361.

Wagner, J.S., Gohm, A. and Rotach, M.W. (2014) The impact of horizontal grid resolution on the boundary layer structure over an idealised valley. *Monthly Weather Review*, 142, 3446–3465. https://doi.org/10.1175/MWR-D-14-00002.1.

Walters, D., Boutle, I., Brooks, M., Melvin, T., Stratton, R., Vosper, S., Wells, H., Williams, K., Wood, N., Allen, T., Bushell, A., Copsey, D., Earnshaw, P., Edwards, J., Gross, M., Hardiman, S., Harris, C., Heming, J., Klingaman, N., Levine, R., Manners, J., Martin, G., Milton, S., Mittermaier, M., Morcrette, C., Riddick, T., Roberts, M., Sanchez, C., Selwood, P., Stirling, A., Smith, C., Suri, D., Tennant, W., Vidale, P.L., Wilkinson, J., Willett, M., Woolnough, S. and Xavier, P. (2017) The Met Office Unified Model global atmosphere 6.0/6.1 and JULES global land 6.0/6.1 configurations. *Geoscientific Model Developments*, 10, 1487–1520. https://doi.org/10.5194/gmd-10-1487-2017.

Walters, D., Baran, A.J., Boutle, I., Brooks, M., Earnshaw, P., Edwards, J., Furtado, K., Hill, P., Lock, A., Manners, J., Morcrette, C., Mulcahy, J., Sanchez, C., Smith, C., Stratton, R., Tennant, W., Tomassini, L., Van Weverberg, K., Vosper, S., Willett, M., Browse, J., Bushell, A., Carslaw, K., Dalvi, M., Essery, R., Gedney, N., Hardiman, S., Johnson, B., Johnson, C., Jones, A., Jones, C., Mann, G., Milton, S., Rumbold, H., Sellar, A., Ujiie, M., Whitall, M., Williams, K. and Zerroukat, M. (2019) The Met Office Unified Model global atmosphere 7.0/7.1 and JULES global land 7.0 configurations. *Geoscientific Model Development*, 12, 1909–1963. https://doi.org/10.5194/gmd-12-1909-2019.

Whiteman, C.D., Bian, X. and Zhong, Z. (1999) Wintertime evolution of the temperature inversion in the Colorado Plateau Basin. *Journal of Applied Meteorology and Climatology*, 38, 1103–1117. https://doi.org/10.1175/1520-0450(1999)038<1103:WEOTTI>2.0.CO;2.

Whiteman, C.D., Zhong, S., Shaw, W.J., Hubbe, J.M., Bian, X. and Mittelstadt, J. (2001) Cold pools in the Columbia basin. *Weather and Forecasting*, 16, 432–447. https://doi.org/10.1175/1520-0434(2001)016<0432:CPITCB>2.0.CO;2.

Wiesenekker, J.M., Kuipers Munneke, P., van den Broeke, M.R. and Smeets, C.J.P.P. (2018) A multidecadal analysis of föhn winds over Larsen C ice shelf from a combination of observations and modeling. *Atmosphere*, 9, 172. https://doi.org/10.3390/atmos9050172.

Wilson, D.R. and Ballard, S.P. (1999) A microphysically based precipitation scheme for the UK Meteorological Office Unified Model. *Quarterly Journal of the Royal Meteorological Society*, 125(557), 1607–1636. https://doi.org/10.1002/qj.49712555707.

Wood, N., Staniforth, A., White, A., Allen, T., Diamantakis, M., Gross, M., Melvin, T., Smith, C., Vosper, S., Zerroukat, M. and Thuburn, J. (2014) An inherently mass-conserving semi-implicit semi-Lagrangian discretization of the deep-atmosphere global non-hydrostatic equations. *Quarterly Journal of the Royal Meteorological Society*, 140(682), 1505–1520. https://doi.org/10.1002/qj.2235.

Xue, H., Li, J., Qian, T. and Gu, H. (2020) A 100-m-scale modelling study of a gale event on the lee side of a long narrow mountain. *Journal of Applied Meteorology and Climatology*, 59, 23–45. https://doi.org/10.1175/JAMC-D-19-0066.1.

Zardi, D. and Whiteman, C.D. (2013) In: Chow, F.K., De Wekker, S.F.J. and Snyder, B. (Eds.) *Diurnal mountain wind systems. In: Mountain Weather Research and Forecasting: Recent progress and current challenges*. Dordrecht Springer, pp. 35–119. https://doi.org/10.1007/978-94-007-4098-3_2.

Zentek, R. and Heinemann, G. (2020) Verification of the regional atmospheric model CCLM v5.0 with conventional data and lidar measurements in Antarctica. *Geoscience Model Development*, 13, 1809–1825. https://doi.org/10.5194/gmd-13-1809-2020.

Zhong, S. and Chow, F.K. (2013) Meso- and fine-scale modeling over complex terrain: parameterizations and applications. In: Chow, F.K., De Wekker, S.F.J. and Snyder, B. (Eds.) *Mountain Weather Research and Forecasting*. Dordrecht: Springer: Springer Atmospheric Sciences. . https://doi.org/10.1007/978-94-007-4098-3_10.

SUPPORTING INFORMATION

Additional supporting information may be found online in the Supporting Information section at the end of this article.

How to cite this article: Orr, A., Kirchgaessner, A., King, J., Phillips, T., Gilbert, E., Elvidge, A. *et al.* (2021) Comparison of kilometre and sub-kilometre scale simulations of a foehn wind event over the Larsen C Ice Shelf, Antarctic Peninsula using the Met Office Unified Model (MetUM). *Quarterly Journal of the Royal Meteorological Society*, 147(739), 3472–3492. Available from: https://doi.org/10.1002/qj.4138